A Bayesian hierarchical model of postlarval delta smelt entrainment: integrating transport, length composition, and sampling efficiency in estimates of loss

Canadian Science Publishing | Canadian Journal of Fisheries and Aquatic Sciences

A Bayesian hierarchical model of postlarval delta smelt entrainment: integrating transport, length composition, and sampling efficiency in estimates of loss

Journal:	*Canadian Journal of Fisheries and Aquatic Sciences*
Manuscript ID	cjfas-2019-0148.R2
Manuscript Type:	Article
Date Submitted by the Author:	30-Oct-2019
Complete List of Authors:	Smith, William; US Fish and Wildlife Service, ; US Fish and Wildlife Service, Newman, Kenneth; Biomathematics and Statistics Scotland, Mitchell, Lara; US Fish and Wildlife Service
Keyword:	entrainment, particle tracking, selectivity, integrated data analysis, Sacramento-San Joaquin Delta
Is the invited manuscript for consideration in a Special Issue? :	Not applicable (regular submission)

A Bayesian hierarchical model of postlarval delta smelt entrainment: integrating transport, length composition, and sampling efficiency in estimates of loss

William E. Smith[1*], Ken B. Newman[2,3], and Lara Mitchell[2]

[1]United States Fish and Wildlife Service, Bay-Delta Office, Sacramento, CA, USA

[2]United States Fish and Wildlife Service, Lodi Office, Lodi, CA, USA

[3]current address: Biomathematics and Statistics of Scotland and School of Mathematics, University of Edinburgh Scotland, UK

[*]corresponding author

email: wes2316@gmail.com

telephone: (915)930-5666

Abstract

Hydrodynamic models have been used to estimate rates of ichthyoplankton transport across marine and estuarine environments and subsequent geographic isolation of a portion of the population, i.e., entrainment. Combining simulated data from hydrodynamic models with data from fish populations can provide more information, including estimates of regional abundance. Entrainment of postlarval delta smelt, a threatened species endemic to California's Sacramento-San Joaquin Delta, caused by water export operations, was modeled using a Bayesian hierarchical model. The model was fit using data spanning years 1995-2015 from multiple sources: hydrodynamic particle tracking, fish length composition, mark-recapture, and count data from entrainment monitoring. Estimates of the entrainment of postlarval delta smelt ranged from 10 (SD=23) in May 2006 to 561,791 (SD=246,423) in May 2002. A simulation study indicated that all model parameters were estimable, but errors in transport data led to biased estimates of entrainment. Using only single data sources rather than integration through hierarchical modeling would have underestimated uncertainty in entrainment estimates or resulted in bias if transport, survival, or sampling efficiency were unaccounted.

Introduction

Entrainment is a physical process whereby groups are advected and spatially redistributed through the action of moving water, resulting in geographic isolation of the entrained portion of the population. Hydrodynamic variation can have profound effects on entrainment of ichthyoplankton, and models that do not account for these hydrodynamics may result in severely biased estimates of entrainment (Blumberg et al. 2004; White et al. 2010). Water movement may be natural (Lough and Manning 2001) or the result of water diversion for human use, such as power generation (Kelso and Milburn 1979) or water extraction (Grimaldo et al. 2009). While natural entrainment plays a role in early dispersal and recruitment in marine and estuarine systems, the typical fate of organisms entrained by water diversions is mortality or removal and isolation from the population. If population losses are substantial, successful management and conservation of populations entrained by water diversions requires an estimation of losses from the population due to the magnitude and variation of entrainment over time (Dixon et al. 2003). For example, the entrainment of fishes into California's South Sacramento-San Joaquin Delta (Fig. 1a) during the process of water extraction and the subsequent mortality of entrained fish has been implicated in the decline of native Sacramento-San Joaquin fish species (USFWS 2008; NMFS 2009). Management of these population requires periodic assessment of past variation in entrainment and the quality of existing biological and environment thresholds used to management the population and to mitigate entrainment effects.

Hydrodynamic models coupled with particle tracking models have been used to simulate egg and larval advection or entrainment through marine (White et al. 2010) and estuarine environments (North et al. 2008; Blumberg et al. 2004). While many studies have estimated rates of entrainment (Boreman et al. 1981) or explored behaviors that modulate entrainment (Culberson et al. 2004), further information can be leveraged by combining transport data with other routinely collected forms of data. For example, population monitoring surveys commonly collect age, length, and abundance information, and mark-

recapture studies often yield information about survival and sampling efficiency. However, such data are rarely integrated with transport data in models of entrainment.

Integrated data analysis is a useful technique for combining information from multiple sources to allow estimation of parameters not identifiable from a single data source (Besbeas et al. 2002), and such analyses are commonly used to model fish population dynamics and assess the status of fish stocks (Methot and Wetzel 2013). Integration of particle tracking data with a population dynamics model of abundance, however, is uncommon. Most studies using particle tracking data to model entrainment do not attempt to estimate abundance but are designed to validate hypothesized interactions between source location, advection, and behavior (Miller 2007); thus, particle tracking data are compared to monitoring data in correlative analyses rather than integrated analyses within a single model (Baumann et al. 2006; Hinckley et al. 2016). Hierarchical modeling is one approach to integrate disparate data types, through use of a multi-level structure (Rochette et al. 2013). Importantly, a hierarchy can facilitate greater statistical power through reduced parameterization and partitioning of errors. A hierarchical approach to modeling abundance of entrained populations can combine independent forms of data in order to model fish population and observation dynamics, such as transport probabilities, survival, length or age composition, and sampling efficiency.

Previous applications of particle tracking data have generally sought to model spatial structure in two or three dimensions, because the initial distribution, or origin, of fish is a critical factor (Heimbuch et al. 2007; Huret et al. 2007) or important hydrodynamic variation occurs in the lateral or vertical dimensions. For example, White et al. (2010) simulated three-dimensional transport of ichthyoplankton in an open coastal system, where water was diverted for power plant cooling. Hydrodynamic complexity in a large open systems creates important 3-dimensional variation in transport, but the volumes of diverted water are very small relative to the volume of the system, and the effect of water diversion on system hydrodynamics is minimal. Conversely, water extraction from smaller riverine systems for irrigation may

represent a much higher volume relative to the system and have a greater impact on hydrodynamics, potentially pulling ichthyoplankton along a simplified linear route. For instance, as much as 35% of inflow to the Sacramento-San Joaquin Delta is exported during April–June (CSWR 1999), and exports rates are often sufficient to reverse the net flows in the two rivers conveying water to the pumps, leading to entrainment events. If the probability of transport from a region of low escapement to sampling locations, e.g., the water diversions, is known, then a simplified 1-dimensional transport model may sufficiently describe net transport without the burden of higher dimensionality. In other words, a model of starting distributions and lateral and vertical dimensions may be unnecessary when transport routes are constrained. Assuming that all fish transported into an entrainment zone are removed from the population, counts at diversions can be used to estimate the number that passed through some downstream region and became entrained. Generally, the abundance of any population being transported or entrained to a set of discrete locations may be estimated from the number arriving at one entrainment location divided by the probability of transport to that location. Alternately, replicated counts of the number arriving at one location can be used to fit a statistical model estimating the number entrained and standard errors. This is, in essence, the N-mixture model, where abundance is estimated from replicate counts and some model of encounter probability (Royle 2004).

Our primary objective was to estimate the number of postlarval fish that entered an area of high entrainment risk and were retained by hydrodynamic conditions. We take advantage of a linear entrainment routing assumption to estimate regional abundance, where regional abundance is considered to reflect eventual entrainment and geographic isolation of a portion of the population. The reduced spatial dimensions of the model avoid the general problems of modeling a starting spatial distribution and transport over longer times and distances. Integration of information about transport, length structure, sampling efficiency, and abundance was achieved using a Bayesian hierarchical model. The hierarchical model structure facilitated a mechanistic description of the sequence of events leading from entrainment to observation, accounting for population dynamic and observation processes. The general purpose of the

model was to explore temporal variation in the number of fish entrained, after accounting for dynamic rates of transport, survival, sampling efficiency and subsampling, and models of each dynamic rate were sufficiently flexible to test covariate effects. The model was applied to estimate regional postlarval abundance of an endangered species, the delta smelt (*Hypomesus transpacificus*), that are entrained during water extraction from the Sacramento-San Joaquin Delta. Water extractions supply more than 25 million people with drinking water (CDWR 2011) and support a $45 billion agricultural industry in California (DFA 2016).

Materials and Methods

The model described below estimated the number of postlarval delta smelt that passed into a region of the South Sacramento-San Joaquin Delta (South Delta) where postlarvae are unlikely to survive, minus the fraction likely to escape entrainment by being transported downstream to a zone of low entrainment risk (the Low Risk Zone; LRZ), based on hydrodynamic conditions. The sequence of events leading from initial entrainment into the South Delta to observation was modeled as a hierarchy of processes that were informed by independent process-specific data sources. Data to estimate components of delta smelt entrainment were noisy and imperfect measures of the processes they represented. Ongoing and proposed research promises to improve data to estimate delta smelt processes in the future, so a flexible modeling framework was developed to accommodate new information as it becomes available, different assumptions, or completely different species and systems.

Study system

Delta smelt are small Osmerid fish endemic to the Sacramento-San Joaquin Delta. Following severe declines in abundance, delta smelt were listed as threatened under the US Endangered Species Act in 1993 and as endangered under the California Endangered Species Act in 2009 (Bennett 2005; CDFW 2018). Entrainment of delta smelt led to issuance of Biological Opinions by the US Fish and Wildlife Service in 2004, 2005, and 2008 that stipulated water operations to minimize entrainment effects

(USFWS 2008). Contentious debate (Kimmerer 2008 and 2011; Miller 2011) and litigation (2010 US District Court ruling) ensued over implementation of the Biological Opinions and management of delta smelt entrainment. Delta smelt entrainment or the population effect of entrainment has been explored by many researchers (Kimmerer 2008; Grimaldo et al. 2009; Maunder and Deriso 2011; Miller et al. 2012; Rose et al. 2013; Kimmerer and Rose 2018) using a variety of statistical methods.

The Sacramento-San Joaquin Delta forms at the confluence of the Sacramento and San Joaquin rivers (Fig. 1A), draining the California Central Valley. The Delta is a network of freshwater tidal sloughs and rivers that acts as a conveyance system for water exported by the Banks and Jones Pumping Plants, located in the southern portion of the Delta (the South Delta) on Old River. Annual export volumes ranged from 2.5 to 8.5 billion m^3 between 1995 and 2014 (ftp://ftp.dfg.ca.gov). High water export rates often reverse the net, or tidally filtered, flows in Old and Middle rivers, and the net upstream flows entrain small fishes into the South Delta. The sum of net Old and Middle River flows (*OMR*) is considered an index of the hydrodynamic forces entraining or drawing delta smelt through the Old and Middle rivers upstream to the water diversions (USFWS 2008). Two fish facilities, operated by the United States Bureau of Reclamation and the California Department of Water Resources, monitor entrainment by screening and removing a fraction of entrained fish (Brown et al. 1996). Large louvers divert fish from intake channels that direct water to the Projects' pumping plants.

Entrainment of delta smelt may be related to seasonal and ontogenetic variation in population distribution and behavior, with different life stages becoming vulnerable to entrainment at different times of year and possibly by different mechanisms. Delta smelt spawning occurs February through May, and postlarvae recruit to the population April through June (Bennett 2005). December through March entrainment of adults may be related to spawning, and some evidence suggests turbidity is related to individual delta smelt behavior, with greater turbidity leading to higher occupancy of mid-channel habitats (Bennett and Bureau 2015), where vulnerability to advective flow is greater. In adults, this behavior may lead to

164 movement upstream, where delta smelt become more vulnerable to entrainment. The east to west
165 distribution of the population in relation to advective flows into the entrainment region may be related to
166 the geographic position of the zone with 0-2 ppt salinity (the Low Salinity Zone) and critical delta smelt
167 habitat (Grimaldo et al. 2009). The Low Salinity Zone moves downstream during the winter, following
168 seasonal rainfall, and then back upstream during the summer as conditions dry. Larval and postlarval life
169 stages may become vulnerable to entrainment when their geographic distribution overlaps the area of
170 South Delta advective flow. The fate of postlarval delta smelt entrained into the South Delta is mortality
171 via direct export from the Delta (Castillo et al. 2012), predation by the robust non-native piscivore
172 community (Clark et al. 2009), thermally induced mortality during the summer (Swanson et al. 1998), or
173 reproductive isolation if fish or their offspring become entrapped by the net southward flows.
174
175 **Data**
176 ***Delta Simulation Model 2 particle tracking data***
177 Transport data to fit the model of delta smelt entrainment consisted of counts of particles that started in a
178 specific region, were transported by simulated hydrodynamics, and were found in a discrete set of regions
179 after a one month period. The particle transport data were used to provide information about the monthly
180 rate at which small fish passed through various regions in the Delta and then arrived at the fish facilities
181 of the State Water (SWP) and Central Valley Projects (CVP) (Table A1). Transport was simulated using
182 California Department of Water Resources's one-dimensional coupled hydrodynamic and particle
183 tracking model, the Delta Simulation Model 2 (DSM2) (CDWR 2013). DSM2 calculates the transport of
184 neutrally buoyant particles in the network of channels comprising the Delta. Simulated transport accounts
185 for important dynamics such as river inflows, water exports, and tidal cycles. For a 21 year period (1995–
186 2015) 4,000 particles were released continuously over a 24-hour period on the first day of April, May, and
187 June into each of three regions of the Delta (Fig. 1B-D). Within each region, particles were inserted at
188 four or five evenly spaced points, and after one month, the individual particle locations were recorded.
189

The final locations were spatially aggregated into regions we designated as sinks, and counts of particles were summed for each region (Table A1-A3). Four sinks were designated, SWP, CVP, Low Risk Zone (LRZ), and Indirect Risk Zone (IRZ). Specifically, we defined the intake channels leading to the export pumps to be the sink locations for SWP and CVP. The LRZ and IRZ were dynamically defined depending upon the source region. The LRZ included areas downstream, north and west of the source region, while the IRZ included remaining regions in the South Delta, generally between the source region and the pumps.

To provide data for a model linking counts at fish facilities to entrainment, for each year-month combination, one of three areas was dynamically selected as an entrainment source region (Fig. 1B-D). Collectively, source regions defined the pathway that entrained fish followed, moving upstream from the San Joaquin River near the mouths of Old and Middle rivers to the SWP and CVP. Source regions represented the downstream edge of a zone of entrainment, which varied as a function of inflow from the Sacramento and San Joaquin rivers and the volume of water exported by the SWP and CVP pumps. The underlying conceptual model was that as inflow volume increased relative to export volume, the area of the region affected by entrainment decreased (Grimaldo et al. 2009), and source regions further away from the pumps were associated with larger areas affected by entrainment compared to source regions near the pumps. The selection of a single source region for each year-month represented a larger or smaller entrainment area, depending on hydrodynamic conditions. Particles (fish) that ended up within or upstream (towards the pumps) of source regions were considered entrained into the South Delta region which included the Old and Middle rivers, portions of the San Joaquin River, and areas adjacent to the SWP and CVP. The three potential source regions, listed here in decreasing distance from SWP and CVP, were: (1) Prisoners Point on the San Joaquin River, (2) Lower Old and Middle rivers, and (3) Upper Old and Middle rivers (Fig. 1B–D). The source region selected for a given year-month combination was the one where the proportion of particles entrained was closest to 0.50, thus the probability of not being

entrained (ending up in the LRZ) was also closest to 0.50. This assumption could be altered to a more or less risk averse decision about probability of entrainment.

The suitability of applying transport probabilities of particles to model delta smelt relied on three assumptions:

1. Postlarval delta smelt experience the same transport processes as passive particles in the DSM2 hydrodynamic model.
2. Fish drawn into the South Delta are effectively removed from the Sacramento-San Joaquin Delta population of delta smelt, and this removal defines entrainment.
3. Entrained fish (through the source region) follow a single linear route into the South Delta, from the Lower San Joaquin River through the Old and Middle rivers to the SWP and CVP pumps, and are not primarily routed through smaller sloughs.

Length composition data

Delta smelt length frequency distributions by year and month were summarized from catch in the 20mm Survey conducted by the California Department of Fish and Wildlife. The 20mm Survey is a monitoring program designed to sample postlarval and juvenile Delta Smelt and covers their historical spring range (CDFW 2019). The 20mm Survey length data from all observations in each month-year combination were used to develop an estimate of the population length composition. Lengths considered in the analysis were restricted to 20–45 mm fork length (i.e., snout to end of center caudal fin ray), where 20 mm is the minimum size enumerated in samples at fish facilities, and 45 mm was the mean bioenergetics growth model prediction (Fujiwara et al. 2005) for the oldest possible postlarvae born March 1. The upper limit excluded larger age-1 fish. Lengths were binned in 5-mm size classes .

Counts and length samples from fish facilities

Delta smelt and other fishes entrained by the SWP and CVP have been routinely monitored since 1979 at the Skinner Fish Facility by the California Department of Water Resources and at the Tracy Fish Facility by the United States Bureau of Reclamation, respectively. As mentioned previously, a fraction of the fish directly entrained in water exports are screened by louvers that divert fish for sampling. These diverted fish at fish facilities are termed salvage in the regional jargon. Since 1993 a subset of diverted fish have been enumerated and measured for length during an approximately 30-minute interval every two hours (Karp et al. 1997). Diverted fish include age-0 and age-1 fish, and fish lengths are used to assign fish ages in the samples.

Mark-recapture data

Delta smelt tagging experiments at the Skinner Fish Facility, which samples fish at the SWP, were reported by Castillo et al. (2012). Six batches of adult delta smelt were tagged with visible implant elastomer and released into the intake channel of Banks Pumping Plant; a fraction was recovered by the Skinner Fish Facility, and the remainder were predated in the intake channel or passed through the louvers and were exported (Table A4). Sutphin and Svoboda (2016) reported on delta smelt tagging experiments at the Tracy Fish Facility, which samples fish at the CVP. Sixty-seven batches of 75 to 400 adult delta smelt were tagged with visible implant elastomer and released in the intake channel of Jones Pumping Plant, and a fraction were later recovered by the Tracy Fish Facility (Table A5). Recoveries of adult tagged fish were assumed to represent samples when length-based louver selectivity equaled one.

Hydrodynamic data

Monthly average OMR was developed from US Geologic Survey streamflow databases for Old River at Bacon Island and Middle River (https://waterdata.usgs.gov).

Model

Motivated by the conceptual model of entrainment described by Kimmerer (2008), we developed a Bayesian hierarchical model of the process leading to the observation of postlarval delta smelt in samples at the SWP and CVP fish facilities between April and June for the years 1995 to 2015. We divided the process into five stochastic sub-processes (Fig. 2): (1) advective transport of fish to the fish facilities, (2) survival of fish during transport, (3) determination of the population length structure, (4) diversion of fish into holding tanks by facility louvers, and (5) subsampling of fish from holding tanks at fish facilities. Sub-processes were modeled as a sequence of probabilities, the product of which was the probability that a fish passing through the source region was observed at the fish facilities. Our primary goal was to estimate the number of postlarval delta smelt at risk of entrainment, either because they entered the facility intake channels or because they were in the South Delta and therefore subject to higher risk of mortality or isolation from the population. A general overview of the model for each sub-process is below, but detailed mathematical descriptions of each sub-process model may be found in Appendix B.

Sub-process 1: Transport of fish to facilities. Transport probabilities $p_{\mathrm{TR}_{qtvs}}$ in year t and month v from the source region q to one of four sinks s (Table 1), or final particle locations (labeled SWP, CVP, LRZ, or IRZ), were estimated from observed particle tracking data. We used a Dirichlet-multinomial model to describe the transport sub-process, where the Dirichlet component accounted for state process variability and the multinomial component accounted for observation error in the particle tracking model data. As previously stated, particle tracking data were generated for three potential source regions (Fig. 1), but only one source region was selected to represent delta smelt transport in a single month. Separate models were fit to each source region's particle tracking data, but only a subset of the probabilities estimated for each source region were applied to delta smelt.

Sub-process 2: Survival. During transport from the source to sink regions and before sampling at fish facilities, fish were exposed to predation, starvation and thermally-induced mortality, also known as pre-screen loss (Gingras 1997; Castillo et al. 2012). No estimates of South Delta mortality exist, but we

hypothesized that mortality during transport to the SWP and CVP was a function of transport time. Longer transport times resulted in greater exposure to predation and higher mortality. Mortality of fish transported to the LRZ was not modeled, and all fish passing through the source region and transported to the IRZ were assumed to be removed from the population. Survival probability $p_{\mathrm{SV1}_{\mathrm{qtv}}}$ for the source region selected as the source for a year-month was applied to all fish arriving at the SWP and CVP.

Additional mortality is experienced by fish going to the SWP. Before entering the SWP intake channel, fish cross a large body of water, Clifton Court Forebay, where they are vulnerable to predation. $p_{\mathrm{SV2}_{\mathrm{tv1}}}$ was the probability of a delta smelt surviving the journey from the Forebay radial gates (where the forebay connects to Old River) to the SWP intake channel in a given year and month. Unlike the other sub-processes in the entrainment model, this sub-process was not directly observed or informed by any data source. Because CVP does not have a forebay, we assumed fish transported to CVP were not subject to this source of mortality and set $p_{\mathrm{SV2}_{\mathrm{tv2}}} = 1$.

Sub-process 3: Population length structure. We modeled the length structure, or length frequency distribution, of the postlarval delta smelt population so we could use this information in the next sub-process, which addresses size selectivity of the louvers. As in the transport sub-process, we used a Dirichlet-multinomial model, where the Dirichlet component modeled the true population length structure $p_{LN_{\mathrm{tvl}}}$, or probability at length *l*, and the multinomial component related delta smelt length frequencies from the 20mm Survey (i.e., the observations) to the population length structure. We divided lengths into five 5mm length classes between 20 and 44mm fork length. We excluded fish 45mm fork length and larger from the 20mm Survey data because delta smelt of this size in spring are likely age 1 and therefore past the postlarval life stage.

316 *Sub-process 4: Sampling efficiency at fish facilities.* The sampling efficiency sub-process handled
317 different aspects of how fish facility gear captured entrained fish and was divided into two sampling
318 probabilities. The fish facility louvers elicit an avoidance behavior that cause entrained fish to move into
319 bypass channels that divert them into holding tanks at the fish facilities. Louvers are spaced
320 approximately 20 mm apart. Delta smelt can easily pass through them. We assumed the louvers were size
321 selective, and that the probability of a delta smelt being diverted increases as fish size increases.
322 Conditional probabilities that a fish in the length sample from the fish facilities is of length l (denoted
323 $p_{\mathrm{BYP}_{\mathrm{tv}l}}$) depended on population length structure $p_{LN_{\mathrm{tv}l}}$ and the length-based selectivity of the louvers p_{SEL_l}.
324 Paralleling the model of observed population length structure, a multinomial model related $p_{\mathrm{BYP}_{\mathrm{tv}l}}$ to
325 length frequencies at the fish facilities.
326
327 $p_{\mathrm{BYP}_{\mathrm{tv}l}}$ reflected the selectivity of the louvers for one length bin relative to the other bins, but not
328 necessarily the overall efficiency of the louvers for diverting fish from the intake channels to the holding
329 tanks. In particular, p_{SEL_l} had an upper asymptote at one, while the maximum efficiency of the louvers for
330 delta smelt of any size is likely less than one. Overall length-specific probabilities of fish being diverted
331 to the fish facilities (denoted $p_{\mathrm{EF}_{lf}}$ for length l and fish facility f) depended on length-based selectivity and
332 maximum sampling efficiency of the louvers estimated from mark-recapture data.
333
334 *Sub-process 5: Subsampling at fish facilities.* The probability of an entrained postlarval fish reaching the
335 fish facility holding tanks was the product of transport probability, survival probability, and sampling
336 efficiency. We treated the total number of delta smelt enumerated in year t and month v at fish facility f,
337 y_{tvf}, as a Poisson random variable,
338
339 (1) $$y_{\mathrm{tvf}} \sim \mathrm{Poisson}\left(n_{\mathrm{S}_{\mathrm{tv}}}\, p_{\mathrm{TRqtvf}}\, p_{\mathrm{SV1}_{\mathrm{tv}}}\, p_{\mathrm{SV2}_{\mathrm{tvf}}} \sum_{l=1}^{5} \left(p_{\mathrm{LN}_{\mathrm{tv}l}}\, p_{\mathrm{EF}_{\mathrm{tvf}l}}\right) \frac{\rho_{\mathrm{tvf}}}{(1-\omega_{\mathrm{tv}})}\right),$$
340

with expected value equal to the estimated number of delta smelt in the holding tank multiplied by the subsampling rate, ρ_{tvf}, and divided by the proportion of fish estimated to be beyond the postlarval stage (namely, 45+mm), $1 - \omega_{\text{tv}}$. $n_{S_{\text{tv}}}$ represented the number that started downstream in the source region. We calculated year-month-facility specific subsampling rates (ρ_{tvf}) as the number of minutes spent sampling fish from the holding tanks divided by the number of minutes during which water was exported; we treated these as fixed values in the model. When subsampling of fish from the holding tanks is carried out, no distinction is made between delta smelt of different life stages. We therefore used the factor $1/(1 - \omega_{\text{tv}})$ to convert our estimate of the number of postlarval delta smelt in the tanks to an estimate of the total number of delta smelt in the tanks, regardless of age.

Number of fish at entrained: We treated the number of delta smelt passing through the source region $n_{S_{\text{tv}}}$ for all months and years, as latent variables. We calculated the number of delta smelt entrained n_{E} as the product of n_{S} and the proportion of those fish that ended up in IRZ, SWP, or CVP (i.e., the proportion of fish that were not transported to LRZ [s = 3]):

$$n_{E_{\text{tv}}} = n_{S_{\text{tv}}}(1 - p_{\text{TR}_{\text{qtv3}}}). \quad (2)$$

Additional details about the estimation of ω_{tv} and about $n_{S_{\text{tv}}}$ priors may be found in Appendix B.

Simulation model and data

The hierarchical Bayesian model for multiple processes was admittedly complex with many parameters. Two sets of simulations were carried out to determine if, or how well, some of the key parameters could be estimated. One set of simulations focused on the estimability of the number entrained n_{E} a parameter of primary interest, via estimability of n_{S}. A considerably reduced statistical model treated the estimated

number of age-0 fish ending up at the SWP and CVP fish facilities and the probabilities of moving from the source to each of the four sinks as known values.

A second simulation study examined estimability of key parameters under a much more complex Bayesian hierarchical model that closely paralleled the one applied to the real data and integrated data from multiple sources. The hierarchical model described above was used to define an operating model, based loosely on the parameters estimated for delta smelt. Random sets of true state dynamics were simulated, then new particle tracking, length composition, and fish facility sample data were stochastically simulated from the set of true states. The estimation model was the same as the operating model; it would therefore fit the simulated data perfectly in the absence of observation error, if all parameters were estimable. The model was then fit to each simulated dataset. Additional simulations focused on the effect of errors in the particle tracking model based probabilities of movement from the source region to the four sinks on posterior distributions of key parameters. Further details regarding each of the two simulation studies may be found in Appendix B.

Model fitting and diagnostics

Weakly informative or uninformative prior distribution were used for all parameters. The model was fit using R package R2jags (Su and Yajima 2015) and the Markov Chain Monte Carlo program JAGS (Plummer 2003). R code to run the model is in Appendix C. Model diagnostics were used to assess convergence, posterior correlations between model parameters, model fit to observations, and posterior predictive distributions. Details regarding priors, fitting and diagnostics can be found in Appendix B.

To explore model robustness, primarily estimation of n_{E}, and to direct future research, data collection, and model refinement, a sensitivity analysis was performed. Sensitivity analyses explored the weighting of transport data, dynamic selection of source regions using empirical values of entrainment probability, Forebay survival estimation (which lacked direct information), the length-based louver selectivity model,

and the value of maximum sampling efficiency, respectively. Model sensitivity to each data component was tested by increasing particle tracking data sample size to 4,000, reducing the potential source regions to just the region nearest the water diversions (Upper Old and Middle River), eliminating the survival model by fixing Clifton Court Forebay survival to 1, eliminating the louver selectivity by fixing selectivity at all lengths to a value of 1, and increasing or decreasing maximum sampling efficiency by 50%. Sensitivity was measured by proportional change in n_{E} from the base model.

Results

Simulation

For the simple multinomial model, which assumed known total recoveries at SWP and CVP and known p_{TR} values, maximum likelihood estimates of n_{S} were unbiased, as expected, and were relatively precise for the given sets of values (Table 2). Assuming that transport was the only source of variation in the number of fish arriving at SWP and CVP, estimability of n_{S} seems a reasonable assumption. This conclusion was reinforced by the second set of more complicated simulations that is discussed next.

The second set of simulations explored estimability of entrainment transport, survival, population length, sampling efficiency and selectivity parameters in the more complex Bayesian hierarchical model. All parameters, including the number of entrained fish, appeared to be estimable using the integrated data analysis and Bayesian hierarchical model described here. We concluded that parameters were estimable if z-scores were between -2 and 2, posterior contraction values were greater than 0, and the 95% coverage of the true value was greater than 0.80 (Table 3), but parameters with right skewed prior distributions (lognormal, gamma, or exponential) were expected to be associated with skewed z-scores. Under conditions of low error in transport data as well as the situation of noisy transport data, estimates of n_{E} were relatively unbiased. Though they appeared estimable from most simulated datasets, regression

parameters for survival β and all errors showed potential for bias, under some conditions, as demonstrated by negative z-scores. The posterior means of the transport random effect σ_{TR} and survival standard error σ_{SV2} were associated with more error compared to other parameters, as indicated by posterior means versus true values (Fig. 3). σ_{SV2} posterior means appeared to be drawn towards the prior means under some conditions, as indicated by a band of posterior σ_{SV2} near the prior mean of 0.22. Negative posterior contraction values for length parameters α_{LN}, σ_{TR}, and σ_{SV2} showed that even simulated data may contain limited information to estimate these values, and posterior distributions for these parameters should be checked to be sure they moved away from the prior distribution.

Under the level of error we simulated in transport data, coverage of most parameters was similar to when no additional error was simulated, but some posterior means of transport parameters appeared to be negatively biased (Table 3). The distribution of z-scores for transport parameters included more negative values when additional transport error was simulated; negative bias in transport parameters was sufficient to reduce the 95% coverage of the true values. As lower values of Dirichlet concentration parameters (transport parameters) are associated with greater uncertainty in Dirichlet-distributed probabilities, probabilities were not necessarily biased, but precision was reduced. The relationship between z-scores and posterior contractions for all parameters appeared to be similar regardless of the simulated level of transport noise.

Model fit to delta smelt data

Estimates of entrainment of postlarval delta smelt (posterior means of n_E; Eq. 14) during 1995–2015 ranged from 561,791 in May 2002 to 10 in May 2006 (Table 4; Fig. 5). Entrainment estimates declined sharply beginning in 2006, and seasonally, the number of postlarvae entrained was greatest in May. Periods with the lowest entrainment estimates were associated with 0s in counts at fish facilities. Coefficients of variation (posterior standard error/posterior mean) for n_E ranged as high as 2.84, reflecting

high uncertainty for some year-month combinations. Model diagnostics indicated that all model parameters converged on stationary posterior distributions, had posteriors with more concentrated distributions than priors, and often different means than the prior distributions (Fig. D2). The integrated model presented here facilitated diagnostic checks on each source of information including fits of the transport model to particle tracking data, population length structure model to 20mm Survey length samples, the selectivity model to length samples at the fish facilities, and the observation model to counts at fish facilities. Specific results for each of the 5 processes are presented below, including summaries of posterior distributions (estimates), residual analyses, goodness of fit (Bayesian P-values), correlation among posterior distributions, and sensitivity analyses.

Transport

Estimates of transport probabilities from the source region to SWP ranged from 6×10^{-5} to 0.66 and transport to CVP ranged 6×10^{-7} to 0.40 (Eq. 1). The effect of OMR on the probability of transport to LRZ (Eq. B2) and the effect of year on transport to the IRZ (Eq. B3) was positive and significantly different from 0 for all months and source regions except Lower Old and Middle rivers (Fig. D3-D5). The year effect on IRZ transport for the Lower Old and Middle rivers source region was not significantly different from 0. Lack of significance was inferred from 95% credible interval coverage of posterior distributions of 0. The model appeared to fit SWP, CVP, and LRZ particle tracking data with little error (Fig. D6), but model fit to IRZ particle tracking data was worse in May and June than in April. In contrast to SWP and CVP data, IRZ transport data were not anchored by observed counts of fish. Bayesian P-values for particle tracking data were between 0.49 and 0.71 for all sink-month combinations (Table 5). Joint posterior correlation of transport parameters with other model parameters was minimal, but some correlation was evident between LRZ and IRZ intercept and slope parameters ($R^2 < 0.58$).

Effective multinomial samples size for the model using particle tracking data converged on an estimate of 225, using the iterative method of McAllister and Ianelli (1997). All analyses were therefore performed

with N_{PT} fixed at 225. Posterior means and coefficients of variation of n_E were sensitive to the value of N_{PT}. When N_{PT} was set equal to 4,000, n_E posterior means decreased 18 to 24% on average (Table 6). Sensitivity analyses suggested that the model was less sensitive to the area selected as a source region in a particular year-month combination. Reducing potential source regions to only the region closest to the SWP and CVP water diversions resulted in 1 to 8% higher n_E posterior means.

Survival to SWP

Survival across Clifton Court Forebay to SWP p_{SV2_1} (Eq. 4) appeared to increase over April–June, with mean survival of 0.03 in April, 0.24 in May, and 0.75 in June. As no direct information was available to estimate this process, most diagnostics were not possible; however, survival parameter posteriors did not appear to be highly correlated with the posteriors of other model parameters. We did not expect that the model of delta smelt survival would be highly informed by the available data, as there was no survival data. Simulation testing indicated that survival error σ_{SV2} may be poorly informed, even with good correspondence between the model and data. Furthermore, model fit to counts at fish facilities was compromised by inclusion of survival process error σ_{SV2}, indicated by very large negative residuals. σ_{SV2} was therefore not estimated, and Eq. 4 was modified to $\text{logit}(p_{SV2_{tv1}}) = \beta_0 + \beta_1 v$. Posterior means of n_E were sensitive to survival estimates, e.g., if p_{SV2_1} was fixed at 1 for all months (and years), estimates of n_E decreased (Table 6). However, the magnitude of the decrease declined from April to June, which makes sense because the estimated values of p_{SV2_1} increase over this period.

Population and fish facility length structure and sampling efficiency

Consistent with a pattern of growth and increasing mean length, the estimated length distribution in the delta smelt population shifted each month from a mode of 20–24 mm fork length in April to a mode of 20–29 mm in May and 30–34 mm in June (Eq. 5). Estimates of the population length distribution accurately fit length distributions from 20mm Survey data; average predicted length compositions

appeared to match up with average observed length compositions (Fig. D8; top panels), and most Bayesian P-values indicated adequate fit to length composition data. P-values for larger length classes in April, however, indicated poor fit (Table 5, 20mm length composition sub-table). Although simulation testing suggested that in the hierarchical model we defined, length parameters could become dominated by their prior distributions, as indicated by negative posterior contraction values, this did not appear to be the case for delta smelt length parameters, which had concentrated posterior distributions that moved away from the priors (Fig. D2).

The model of louver selectivity indicated that the smallest fish, 20-24 mm fork length, had a 0.74 probability of being sampled given contact with the louvers (Eq. 9). The slope of the selectivity model (η_0) was high, and by 30-34 mm fork length, fish appeared to be fully selected. Model diagnostics indicated somewhat worse fit of the louver selectivity model in June. Mean observed length frequencies at fish facilities were captured within 95% credible intervals (i.e., residuals spanned zero) for April and May but not for the largest length class in June (Fig. D8; bottom panels). High June P-values also indicated poor fit to the largest length classes observed in June at the fish facilities. The selectivity model parameter, η_1, was not correlated with other model parameters, and posterior means and coefficients of variations of n_{E} did not appear to be sensitive to the louver selectivity model (p_{SEL}; Table 6).

Simulation testing indicated that biases could arise when all transport, survival and efficiency errors were simultaneous estimated, at least when survival data were missing, which is the current situation for postlarval delta smelt. As was stated previously, the mark-recapture model was fit externally, and maximum sampling efficiency parameters Γ_{f} and $\sigma_{\mathrm{EF_f}}$ were treated as fixed values, with mean SWP efficiency of 0.52 and mean CVP efficiency of 0.17 (Eq. 12) . Estimates of n_{E} were sensitive to the value assumed for Γ_{f} (Table 6). Lower values resulted in higher estimates of n_{E}, and higher values of Γ_{f} resulted in lower estimates of n_{E}.

517

518 ***Subsampling at fish facilities***

519 Overall, the model appeared to accurately predict observed counts at fish facilities. While residuals did
520 indicate a pattern of overestimation of counts at the CVP fish facility (Fig. D7), the medians of all
521 standardized residuals were between 2 and -2. Further, the 95% credible intervals of most standardized
522 fish facility count residuals contained 0. The largest residuals occurred at low values of predicted
523 entrainment, and the highest counts at fish facilities were accurately estimated by the model. Bayesian P-
524 values indicated particularly good and consistent fit to CVP data in all months, while the fit to SWP fish
525 facility counts was worst in April but improved in May and June (Table 5, counts at fish facilities sub-
526 table).

527

528 **Discussion**

529

530 We developed a Bayesian hierarchical model that integrated several sources of information about the
531 entrainment, transport, population length structure and sampling efficiency of postlarval fish. The
532 fundamental property of the hierarchical framework was that some parameters were functions of other
533 parameters. Integration was achieved because parameters were shared among multiple sub-processes. A
534 hierarchy linked data across sub-processes, linked observation models to state process models and
535 facilitated a reduced parameterization when covariates were available. The formulation of process models
536 as linked general linear models (transport and survival) facilitated tests of covariates hypotheses. The
537 hierarchical structure allowed simultaneous accounting of process variation and sampling uncertainty
538 when estimating the abundance of entrained fish. Process variation and observation error can be difficult
539 to disentangle (de Valpine and Hilborn 2005), and this complication may have manifested in the observed
540 tradeoffs between the fit to particle tracking data and counts at fish facilities. Although it is possible to
541 develop a non-hierarchical model that integrates abundance and entrainment estimation, the hierarchical

542 structure provided a clearer accounting of which process uncertainties were represented in estimates of
543 entrainment.
544
545 The inclusion of multiple data sets, in an integrated analysis, meant that information about the abundance
546 of entrained fish came from multiple sources, and integration of mechanistic transport data from
547 hydrodynamics modeling, direct information about sampling efficiency from mark-recapture studies, and
548 observed counts at fish facilities (sometimes viewed as an index of entrainment) leveraged those data
549 sources against each other. The transport data from particle tracking, for example, provided a measure of
550 movement not contained in other data sets, while counts from SWP and CVP fish facilities adjusted the
551 particle tracking-based transport probabilities and scaled the entrainment estimates. In a sense, the fitted
552 model may be viewed as a calibration of the model provided by particle tracking, and lack of fit, such as
553 the larger May and June particle tracking residuals for the Low and Indirect Risk Zones, may represent
554 instances where particle tracking data was not representative of fish transport. Goodness of fit testing on
555 multiple data sets, within the integrated framework provided a framework to assess those deficiencies and
556 update entrainment estimates should new information become available. Even with hierarchical modeling,
557 some ambiguity remains for delta smelt entrainment because some critical processes were poorly
558 informed by available data (e.g. no survival data). While these data insufficiencies compromised delta
559 smelt estimates, they also demonstrated the benefits of integrating the estimation of several model
560 components and provided a basis to prioritize future data collection.
561
562 ***Modeling the spatial structure of entrainment***
563 Models to estimate entrainment have been applied to three general settings which differ in terms of how
564 spatial structure is handled. In one setting, individual origins are important, necessitating spatially
565 resolved population models and two- or three-dimensional hydrodynamic modeling (White et al. 2007).
566 In a second setting, entrainment occurs through a complex environment that requires three-dimensional
567 hydrodynamic modeling (Heimbuch et al.2007). Finally, in a third setting and the one presented here,

spatial origins are less important and entrainment occurs through a simplified network of channels allowing non-spatial population models and lower hydrodynamic dimensionality (Kimmerer 2008). While complex coastal and estuarine hydrodynamics (the second setting) may require three-dimensional modeling to achieve suitable accuracy, movement of water through linear riverine systems can be viewed as a special case of the third setting and can be accurately modeled in one dimension. For example, the California Department of Water Resources uses the one-dimensional hydrodynamic model DSM2 to evaluate flood risk and manage water transfers (CDWR 2013), and DSM2 has been considered an accurate transport model for early lifestages of delta smelt (Rose et al. 2013; Kimmerer and Rose 2018).

Transport through a single region per time period was modeled in order to avoid spatially stratifying the sources regions of entrained fish and to reduce the distance over which transport was modeled. Rather than estimating transport from multiple regions, the process of delta smelt transport was assumed to be linearly routed through a single region, extending from the Lower San Joaquin River and up the Old and Middle River corridor to the water diversions. The routing assumption was justified by the fact that only smaller sloughs intersect with the corridor between the SWP and CVP and the confluence with the San Joaquin River. At the head of Old River or the San Joaquin River upstream of Stockton, delta smelt are rarely captured in monitoring surveys, so it is unlikely that many delta smelt arrive at the SWP and CVP from upstream locations. While restricting the geographic extent of space to just the entrainment routes through the South Delta facilitated a model of transport over relatively short durations, during periods of lesser upstream flow, this advantage was reduced. Based on ad hoc estimates of transport time calculated from the shortest route from the mouth of Old River to the CVP, mean channel area from DSM2 documentation (CDWR 2013), and Old and Middle River flow rate during the study period, transport through the Old and Middle River corridor occurred at the scale of days during most of the study period. In situations where entrainment probability was greatest (i.e., high water velocities and strong upstream Old and Middle River flows), transport occurred over a short duration. If errors in a hydrodynamic model of transport increase proportionally to transport time because fish have longer to modify their transport

with behaviors, then higher downstream flows, lower entrainment probabilities, and corresponding longer transport times are associated with greater error in a one-dimensional particle tracking model of delta smelt transport. Reducing the subset of potential source regions to areas closer to sampling locations could reduce potential unmodeled interactions between transport time and fish behavior.

Among the three potential source regions, the region for a particular year-month was selected such that the probability of transport to the Low Risk Zone was close to 0.5, relative to the other potential source regions. Selection of source region influenced estimates of entrainment; sensitivity analysis demonstrated that reduction of source regions to areas near the pumps resulted in lower entrainment estimates during most periods. Transport probabilities to the SWP and CVP are higher in areas closer to the diversions, and probabilities of transport to the Indirect Risk Zone are lower, compared to areas further downstream. The effect of changing source regions was relatively minor, however, compared to the effects of changing effective sample size (weighting of particle tracking data), assumed survival rate, or estimates of sampling efficiency.

Alternate models, data needs, and further work

An important modeling choice was whether to treat transport data as multinomial random observations or as covariates. The distinction between these alternatives was how error was handled. As an observation, transport data are subject to observation error, and this was structured into the state-observation hierarchy of the transport model. As a covariate, transport data could be treated as a predictor in a log-linear Dirichlet regression model, with transport probability as the response; however, linear models generally assume that predictors are measured without error. By treating transport information as an observation, we were able to partially account for the errors in a hydrodynamic model of transport lacking fish behavior.

Our choice of Dirichlet-multinomial models to describe transport and length observations, given a set of probabilities, introduced a critical uncertainty. Though known quantities of transported particles and fish lengths were sampled, the effective sample sizes were unknown. The multinomial model assumes each observation is independent, but correlations among observations arise from sampling particles released during the same time period or fish lengths measured from groups caught in surveys, resulting in uncertainty in effective multinomial sample sizes. Effective sample sizes were an unknown quantity but can be estimated either externally to the model fitting step, as we did for transport data, (McAllister and Ianelli 1997), or internally as a component of the model likelihood (Thorson et al. 2017). A traditional "rule of thumb" that we applied to length samples, is to set effective sample size equal to the number of independent units from which lengths were sampled, such as number of tows. A final option is to avoid the reweighting associated with choosing an effective sample size by modeling proportions rather than counts (Francis 2017).

Although we make the argument that one-dimensional hydrodynamic modeling is suitable to model postlarval fish transport, two- or three-dimensional models could be applied to develop transport data and estimate entrainment. During periods of high water export volumes (e.g., as much as 35% of inflow during April–June [CSWR 1999]), advective forces from pumping may dominate transport, but during periods of lower flows, tidal forces dominate the region where delta smelt are entrained. Three-dimensional hydrodynamic modeling may be required to simulate complex tidal mixing (Sridharan et al. 2018). Coding particles with hypothesized fish behaviors in coupled hydrodynamics-particle tracking models is a common approach to modeling marine entrainment (Miller 2007). The model presented here is sufficiently flexible to incorporate such information; only numbers of particles reaching a subset of sinks is required for the model to estimate transport rates and entrainment.

We made simplifying assumptions about the spatiotemporal scale of entrainment, modeling a monthly time interval and transport from only a single source region. A time series approach could be used to

model both finer temporal and spatial scales. An entrainment model could be specified to account for the dependence of sequential abundances using a time series in which abundances are linked by survival and regional abundance at time *t* is equal to abundance times survival from time *t*-1 plus movement from other regions. A time series can be used to leverage entrainment estimates at a finer temporal resolution if only starting abundances need to be estimated. Postlarval delta smelt, however, recruit to the population during the seasonal period we modeled. Postlarval abundance at *t* does not necessarily depend on abundance at *t*-1, and if abundance must be estimated in each time period, the temporal scale must be coarse in order to reduce the number of abundances to estimate. Important variation in hydrodynamics, related for example to acute storm events, is certainly lost.

Using a time series approach and more highly resolved transport information, a spatially-explicit model (a special case of the first spatial structure setting mentioned above) could estimate spatially stratified abundance for the entire population, then apply strata-specific transport rates to sampling locations. The drawback to a spatially-explicit approach is that starting population distributions may be highly uncertain (Heimbuch et al. 2007; Huret et al. 2007; Simonis and Merz 2019). Further, any biases in the transport model (e.g., unaccounted fish behavior) compound over both time and space, because fish transport over longer distances must be modeled. For example, few delta smelt are currently captured in monitoring surveys due to low abundance, resulting in imprecise estimates of spatial distributions (USFWS 2018), from which unknown behaviors may modify transport over distances of more than 80 km during the process of entrainment. In the single-region approach we applied, transport assumptions were applied over shorter distances of up to 35 km during low outflow and less than 15 km at high outflow.

An alternative for modeling transport using particle tracking data would make use of information about fish origins collected from entrained fish observed at fish facilities. Though such information does not currently exist for delta smelt, otolith microchemistry, tagging or genetic data have been used to assign spatial origins to other larval or juvenile fishes. Counts of the number of fish observed at fish facilities,

671 mapped to a set of starting locations, could be used to develop a model paralleling that for transport
672 probabilities and particle tracking data, where Dirichlet-distributed probabilities represent a starting
673 spatial structure times transport probabilities and counts at fish facilities are multinomially distributed into
674 a discrete set of origins.
675
676 We assumed that the group of fish entrained was reset at the beginning of each month, with all fish that
677 entered the South Delta being directly entrained by the SWP and CVP water export pumps, escaping
678 entrainment by being transported back to the Low Risk Zone, or becoming isolated in the South Delta
679 where they eventually died. Future refinements to the model presented here could account for entrained
680 fish that did not die, because they were transported to the Indirect Risk Zone rather than the SWP or CVP,
681 and were then available to be sampled in the subsequent time period, although their entrainment occurred
682 earlier. Transport of Indirect Risk Zone fish can be modeled like entrained fish, using a Dirichlet-
683 multinomial model with the Indirect Risk Zone as the source region of particle tracking data. Numbers
684 available for observation would be the product of the number previously entrained and the joint
685 probability of survival and transport. Particle tracking data for two consecutive one month periods would
686 be required, because the transport of entrained fish from the Indirect Risk Zone at time *t* depends on their
687 spatial distribution within the Indirect Risk Zone at *t*-1. We were limited in the present study by particle
688 tracking of only one month at a time. Further, available data to model transport were counts of particles
689 released on the first day of each month and tracked until the last day of the month, making them an
690 imperfect index of the continuous process of transport over each month (Culberson et al. 2004; Kimmerer
691 and Nobriga 2008). A preferable strategy would release particles more evenly throughout the month then
692 track them through the end of the subsequent month.
693
694 Sensitivity and simulation testing suggested the model was sensitive to transport, survival, and maximum
695 sampling efficiency but less sensitive to length-based selectivity. This result suggests that more or better
696 delta smelt selectivity information is unlikely to change entrainment estimates but improved delta smelt

transport, survival, and maximum sampling efficiency information may be beneficial. In more than ten years since the publication of the first model of delta smelt entrainment (Kimmerer 2008), statistical models have advanced, but little new data to estimate parameters critical to delta smelt entrainment have been collected. Nevertheless, we outline future research to improve the entrainment estimates presented here. The residual pattern of more negative CVP residuals in June suggested a conflict between counts from fish facilities and transport data provided by particle tracking. We expected that as fish progressed to later lifestages, behavioral development would decouple observed transport in counts at fish facilities from hydrodynamics and observed transport in particle tracking data. Further, simulation testing indicated that the precision of entrainment estimates in the Bayesian hierarchical framework were sensitive to errors in transport data; the estimates were only as good as the information provided by particle tracking data. The high standard deviation associated with modeled postlarval delta smelt survival may be symptomatic of this relationship. Research linking ontogenetic development of behaviors in response to environmental cues and transport may help to disentangle these model components in the future.

Sensitivity analyses revealed that the model was sensitive to the maximum value of sampling efficiency and survival of fish to the SWP (also known as pre-screen loss). Sparse data have been collected to estimate these parameters. Prior research into survival and efficiency was exploratory (Castillo et al. 2012), and similar, more focused mark-recapture research is warranted to improve estimates of postlarval delta smelt entrainment. Although we did not model additional mortality for fish transported to the CVP, it is possible that fish experience elevated mortality in the CVP intake channels, analogous to survival in Clifton Court Forebay, before becoming available for observation. Mark-recapture data to estimate survival in Clifton Court Forebay and the intake channels exist for adults and may be used to directly estimate survival of entrained adult delta smelt rather than the indirect methods we used (Smith 2019). Survival during transport to the SWP and CVP was a function of transport time and the daily mortality rate estimated by Bennett (2005), but other models of mortality are possible. Our assumed mortality model was necessary because no estimates of delta smelt mortality in the South Sacramento-San Joaquin

Delta exist. We make the strong assumption that all fish entering the Indirect Risk Zone that are not transported back to the Low Risk Zone within one month die. Fish transported back to the Low Risk Zone may experience elevated mortality while in the South Delta, but we cannot account for exposure time to elevated mortality or what that elevated mortality may be. Although particle tracking information accounts for variation in transport due to flow, exports, and tidal cycles, information was not retained about the length of time particle were in the South Delta before returning to the Low Risk Zone.

Mark-recapture studies could also help to refine the model of length-based louver selectivity. Sensitivity analyses, however, suggested that delta smelt entrainment estimates were not sensitive to selectivity. Low numbers of delta smelt are captured in existing monitoring surveys and fish facility samples, resulting in difficulty estimating population length and selectivity parameters. Model insensitivity to selectivity may be related to the relatively high slope of the fitted selectivity model (η_0). After the first length class, selectivity to the gear was constant, so changing selectivity only affected values from the first length class. In scenarios with more length classes having lower selectivity, estimates of entrainment may become more sensitive to selectivity estimates.

Conclusions

To better guide management decisions made to protect and restore the delta smelt population, estimates of entrainment will be integrated with abundance estimates and errors in the US Fish and Wildlife Service's Delta Smelt Life Cycle Model. Features of the model include a state-space formulation to separate observation errors from stochasticity in survival and reproduction, a time-series approach that smooths over multiple life stages, and formulation using managed environmental quantities. Modeling numbers of entrained fish estimated here as a function of per capita entrainment rates, the hypothesis that past conservation actions changed rates of loss due to entrainment can be tested. Although we estimated large declines in the number of delta smelt postlarvae entrained beginning around the time of implementation of conservation actions by the US Fish and Wildlife Service to reduce entrainment losses, in years 2007

749 and 2008, the overall delta smelt population was also in severe decline at the same time (Moyle et al.
750 2016; Polansky et al. 2019). A population dynamics model that includes survival and reproduction is
751 needed to separate the effects of abundance from entrainment. The accuracy and power of the Delta Smelt
752 Life Cycle Model to detect changes in vital rates depends on the accounting of observation errors
753 described in the current model. Ultimately, this work will aid in the development and assessment of
754 environmental criteria to manage and recover the delta smelt population.
755
756 Entrainment of ichthyoplankton through aquatic systems is a complex function of system hydrodynamics,
757 but sophisticated biophysical models coupling hydrodynamics and particle tracking can provide
758 information about transport rates. Bayesian hierarchical modeling provides a useful tool for integrating
759 models for a sequence of events with disparate datasets that partially inform dynamics of the sequence.
760 With these tools and admittedly strong assumptions about how entrained fish were routed through the
761 system, we demonstrated the possibility of estimating entrainment as the regional abundance of a pelagic
762 postlarval fish while accounting for complex but common sources of variation.
763
764 While past models of entrainment have focused on more complex transport dynamics in marine and
765 estuarine systems, water extraction from a riverine system with more or less linear flow dynamics
766 presents opportunities to make simplifying assumptions about the dimensionality of transport. It is
767 particularly convenient to assume that entrainment follows a linear route through a single region,
768 requiring only a one-dimensional transport model and no assumptions about population starting
769 distributions. With several existing high volume water diversions throughout the U.S. and Canada
770 (Lasserre 2007), many more recently completed or planned in developing areas like
771 Africa (Gereta et al. 2002), China (Wei 2005), and Brazil (Molisani et al. 2006), and growing global
772 demand for freshwater resources, the impacts of water extraction on aquatic populations are likely to
773 increase. Conservation of these aquatic systems and mitigation of impacts from water extraction will

774 require accurate quantification of entrainment losses and a mechanistic model of loss rates as a function
775 of altered hydrodynamics.
776
777 **Acknowledgements**
778
779 The findings and conclusions in this article are those of the authors and do not necessarily represent the
780 views of the US Fish and Wildlife Service. Gonzalo Castillo, Li-Ming He, Matt Nobriga, and Leo
781 Polansky kindly provided reviews of early drafts this manuscript, and suggestions from Wim Kimmerer
782 and four anonymous reviewers substantially improved the article's quality. Luisa Studen and Elden
783 Holldorf provided GIS mapping support. Funding was provided under the Delta Smelt Life Cycle Model
784 contract with the California Department of Water Resources.
785
786 **References**
787
788 Baumann, H., Hinrichsen, H-H., Möllmann, C., Köster, F.W., Malzahn, A.M., and Temming, A. 2006.
789 Recruitment variability in Baltic Sea sprat (Sprattus sprattus) is tightly coupled to temperature and
790 transport patterns affecting the larval and early juvenile stages. Can. J. Fish. Aquat. Sci. **63**: 2191–
791 2201. doi:10.1139/f06-112.
792
793 Bennett, W.A. 2005. Critical assessment of the delta smelt population in the San Francisco Estuary,
794 California. San Francisco Estuary Watershed Sci, 3. Available from:
795 https://escholarship.org/uc/item/0725n5vk.
796

Bennett, W.A. and Burau, J.R. 2015. Riders on the storm: selective tidal movements facilitate the spawning migration of threatened Delta Smelt in the San Francisco Estuary. Estuaries and Coasts **38**(3): 826–835. doi: 10.1007/s12237-014-9877-3.

Besbeas, P., Freeman, S.N., Morgan, B.J., and Catchpole, E.A. 2002. Integrating mark–recapture–recovery and census data to estimate animal abundance and demographic parameters. Biometrics **58**: 540–547. doi: 10.1111/j.0006-341X.2002.00540.x.

Blumberg, A. F., Dunnin, D. J., Li, H., Heimbuch, D., and Geyer, W. R. 2004. Use of a particle-tracking model for predicting entrainment at power plants on the Hudson River. Estuaries **27**: 515–526. doi:10.1007/BF02803543.

Blumberg, A., Goodwin, P., Houde, E., Monismith, S., and Powell, T. M. 2010. Review of IEP and other Bay-Delta modeling focused on hydrodynamics and fish, Interagency Ecological Program. Available from: http://www.dwr.water.ca.gov/iep/docs/IEPModelWorkshopReview.pdf

Boreman, J., Goodyear, C.P., and Christensen, S.W. 1981. An empirical methodology for estimating entrainment losses at power plants sited on estuaries. Trans. Am. Fish. Soc. **110**: 253–260. doi: 10.1577/1548-8659(1981)110<253:AEMFEE>2.0.CO;2.

Brown, L. R., Greene, S., Coulston, P., and Barrow, S. 1996. An evaluation of the effectiveness of fish salvage operations at the intake to the California Aqueduct, 1979–1993. *In* San Francisco Bay: the Ecosystem. *Edited by* J. T. Hollibaugh. American Association for the Advancement of Science, Pacific Division, San Francisco, C.A. pp 497–518

California Department of Agriculture (DFA). 2016. California agricultural production statistics [online]. Available from: https://www.cdfa.ca.gov/statistics/

California Department of Fish and Wildlife (CDFW). 2018. State and federally listed threatened and endangered animals of California. Available from: https://nrm.dfg.ca.gov/FileHandler.ashx?DocumentID=109405

California Department of Fish and Wildlife (CDFW). 2019. 20mm survey project overview [online]. Available from: https://www.dfg.ca.gov/

California Department of Water Resources (CDWR). 2011. California State Water Project at a glance [online]. Available from: https://www.water.ca.gov/-/media/DWR-Website/Web-Pages/What-We-Do/Infrastructure/Files/Publications/Californias-State-Water-Project-at-Glance.pdf

California Department of Water Resources (CDWR). 2013. Delta Simulation Model II [online]. Available from: http://baydeltaoffice.water.ca.gov/modeling/deltamodeling/models/dsm2/dsm2.cfm.

California State Water Resources Control Board (CSWR). 1999. Water right decision D-1641. California Environmental Protection Agency, Sacramento, CA, USA.

Castillo, G., Morinaka, J., Lindberg, J., Fujimura, R., Baskerville-Bridges, B., Hobbs, J., Tigan, G. and Ellison, L. 2012. Pre-screen loss and fish facility efficiency for delta smelt at the south Delta's State Water Project, California. San Francisco Estuary Watershed Sci. **10**(4). Available from: https://cloudfront.escholarship.org/dist/prd/content/qt28m595k4/qt28m595k4.pdf.

847 Clark, K.W., Bowen, M.D., Mayfield, R.B., Zehfuss, K.P., Taplin, J.D., and Hanson, C.H. 2009.
848 Quantification of pre-screen loss of juvenile steelhead in Clifton Court Forebay, State of California,
849 Sacramento. California Department of Water Resources, Sacramento, CA, USA.
850
851 Culberson, S. D., Harrison, C.B., Enright, C., and Nobriga, M.L. 2004. Sensitivity of larval fish transport
852 to location, timing, and behavior using a particle tracking model in Suisun Marsh, California. Am.
853 Fish. Soc. Symp. **39**: 257–268. Available from:
854 http://www.water.ca.gov/aes/docs/Culberson_et_al_2004.pdf.
855
856 Dixon, D., Veil, J.A., and Wisniewski, J. 2003. Defining and assessing adverse environmental impact
857 from power plant impingement and entrainment of aquatic organisms: symposium in conjunction
858 with the annual meeting of the American Fisheries Society, 2001, in Phoenix, Arizona, USA. CRC
859 Press, Boca Raton, F.L.
860
861 de Valpine, P.D. and Hilborn, R. 2005. State-space likelihoods for nonlinear fisheries time-series. Can. J.
862 Fish. Aquat. Sci. **62**: 1937–1952. doi: 10.1139/f05-116.
863
864 Francis, R. C. (2011). Data weighting in statistical fisheries stock assessment models. Can. J. Fish. Aquat.
865 Sci. **68**: 1124–1138. doi: 10.1139/f2011-025.
866
867 Francis, R.C. 2017. Revisiting data weighting in fisheries stock assessment models. Fish. Res. **192**: 5–15.
868
869 Fujiwara, M., Kendall, B.E., Nisbet, R.M., and Bennett, W.A. 2005. Analysis of size trajectory data using
870 an energetic-based growth model. Ecology **86**(6): 1441–1451. doi: 10.1890/04-1351.
871

872 Gereta, E., Wolanski, E., Borner, M., and Serneels, S. 2002. Use of an ecohydrology model to predict the
873 impact on the Serengeti ecosystem of deforestation, irrigation and the proposed Amala Weir Water
874 Diversion Project in Kenya. Int. J. Ecohydrology Hydrobiology **2**: 135–142.
875
876 Gingras, M. 1997. Mark/recapture experiments at Clifton Court Forebay to estimate pre-screening losses
877 to juvenile fishes 1976–1993. Interagency Ecological Program Technical Report 55. Available from:
878 http://www.water.ca.gov/iep/products/technicalrpts.cfm.
879
880 Grimaldo, L.F., Sommer, T., Van Ark, N., Jones, G., Holland, E., Moyle, P.B., Herbold, B., and Smith, P.
881 2009. Factors affecting fish entrainment into massive water diversions in a tidal freshwater estuary:
882 can fish losses be managed? N. Am. J. Fish. Manage. **29**: 1253–1270. doi:10.1577/M08-062.1.
883
884 Heimbuch, D.G., Dunning, D.J., Ross, Q.E., and Blumberg, A.F. 2007. Assessing potential effects of
885 entrainment and impingement on fish stocks of the New York–New Jersey Harbor estuary and Long
886 Island Sound. Trans. Am. Fish. Soc. **136**: 492–508.
887
888 Hinckley, S., Parada, C., Horne, J.K., Mazur, M. and Woillez, M. 2016. Comparison of individual-based
889 model output to data using a model of walleye pollock early life history in the Gulf of Alaska. Deep-
890 Sea Res. Pt. II **132**: 240–262. doi:10.1016/j.dsr2.2016.04.007.
891
892 Huret, M., Runge, J.A., Chen, C., Cowles, G., Xu, Q. and Pringle, J.M. 2007. Dispersal modeling of fish
893 early life stages: sensitivity with application to Atlantic cod in the western Gulf of Maine. Marine
894 Ecology Progress Series **347**: 261–274. doi: 10.3354/meps06983.
895
896 Karp, C., Hess, L., Lyons, J., and Liston, C. 1997. Evaluation of the sub-sampling procedure to estimate
897 fish salvage at the Tracy Fish Collection Facility, Tracy, California, 1993-1996. Tracy Fish Collection

898 Facility Studies, Volume 8. United States Bureau of Reclamation, Mid-Pacific Region and Denver
899 Technical Service Center, Denver, C.O. Available from: https://www.usbr.gov/mp//TFFIP/technical-
900 reports.html.
901
902 Kelso, J.R. and Milburn, G.S. 1979. Entrainment and impingement of fish by power plants in the Great
903 Lakes which use the once-through cooling process. J. Great Lakes Res. **5**: 182–194.
904 doi:10.1016/S0380-1330(79)72145-9.
905
906 Kimmerer, W.J. 2008. Losses of Sacramento River Chinook salmon and delta smelt to entrainment in
907 water diversions in the Sacramento–San Joaquin Delta. San Francisco Estuary and Watershed Sci.
908 **6**(2).
909
910 Kimmerer, W.J. 2011. Modeling Delta Smelt losses at the south Delta export facilities. San Francisco
911 Estuary and Watershed Sci. **9**(1).
912
913 Kimmerer, W.J. and Nobriga, M.L. 2008. Investigating Particle Transport and Fate in the Sacramento-San
914 Joaquin Delta Using a Particle-Tracking Model. San Francisco Estuary and Watershed Sci. **6**(1).
915 Available from: https://cloudfront.escholarship.org/dist/prd/content/qt547917gn/qt547917gn.pdf.
916
917 Kimmerer, W.J. and Rose, K.A. 2018. Individual-Based Modeling of Delta Smelt Population Dynamics
918 in the Upper San Francisco Estuary III. Effects of Entrainment Mortality and Changes in Prey. Trans.
919 Am. Fish. Soc. **147**(1): 223–243.
920
921 Korman, J., Gross, E.S., Smith, P.E., Saenz, B., and Grimaldo, L. *In prep*. Statistical evaluation of
922 particle-tracking models predicting proportional entrainment loss for adult delta smelt in the
923 Sacramento-San Joaquin Delta.

Lasserre, F. 2005. Massive water diversion schemes in North America: a solution to water scarcity? WIT Transactions on Ecology and the Environment **80**. Available from: https://www.witpress.com/Secure/elibrary/papers/WRM05/WRM05039FU.pdf

Lough, R.G. and Manning, J.P. 2001. Tidal-front entrainment and retention of fish larvae on the southern flank of Georges Bank. Deep-Sea Res. Pt. II **48**: 631–644. doi:10.1016/S0967-0645(00)00130-2.

Mager R., Doroshov, S.I., Van Eenennaam, J.P., and Brown, R.L. 2004. Early life stages of delta smelt. In: Freyer, F., L. R. Brown, R. L. Brown, J. J. Orsi, editors. Early life history of fishes in the San Francisco estuary and watershed. Am. Fish. Soc. Symp. **39**: 169–180.

Maunder, M.N. and Deriso, R.B. 2011. A state–space multistage life cycle model to evaluate population impacts in the presence of density dependence: illustrated with application to delta smelt (Hyposmesus transpacificus). Can. J. Fish. Aquat. Sci. **68**(7): 1285–1306. doi: 10.1139/f2011-071.

McAllister, M.K. and Ianelli, J.N. 1997. Bayesian stock assessment using catch-age data and the sampling-importance resampling algorithm. Can. J. Fish. Aquat. Sci. **54**(2): 284–300.

Miller, T.J. 2007. Contribution of individual-based coupled physical–biological models to understanding recruitment in marine fish populations. Mar. Ecol. Prog. Ser. **347**: 127–138.

Miller, W J. 2011. Revisiting assumptions that underlie estimates of proportional entrainment of delta smelt by state and federal water diversions from the Sacramento-San Joaquin Delta. San Francisco Estuary and Watershed Sci. **9**(1).

Miller, W. J., Manly, B. F., Murphy, D. D., Fullerton, D., & Ramey, R. R. (2012). An investigation of factors affecting the decline of delta smelt (Hypomesus transpacificus) in the Sacramento-San Joaquin Estuary. Rev. in Fish. Sci. **20**(1): 1–19.

Methot, R.D. and Wetzel, C.R. 2013. Stock synthesis: a biological and statistical framework for fish stock assessment and fishery management. Fish. Res. **142**: 86–99. doi:10.1016/j.fishres.2012.10.012.

Molisani, M.M., Kjerfve, B., Silva, A.P., and Lacerda, L.D. 2006. Water discharge and sediment load to Sepetiba Bay from an anthropogenically-altered drainage basin, SE Brazil. J. Hydrology **331**: 425–433.

Moyle, P.B., Brown, L.R., Durand, J.R. and Hobbs, J.A. 2016. Delta smelt: life history and decline of a once-abundant species in the San Francisco Estuary. San Francisco Estuary and Watershed Sci. **14**(2).

Newman, K.B., Buckland, S.T., Morgan, B.J., King, R., Borchers, D.L., Cole, D.J., Besbeas, P., Gimenez, O., and Thomas, L. 2014. Modelling population dynamics: model formulation, fitting and assessment using state-space methods. Springer, New York City, N.Y.

National Marine Fisheries Service (NMFS). 2009. Biological opinion on long-term operations of the Central Valley Project and State Water Project. Available from: https://www.westcoast.fisheries.noaa.gov/publications/Central_Valley/

North, E.W., Schlag, Z., Hood, R.R., Li, M., Zhong, L. Gross, T., and Kennedy, V.S. 2008. Vertical swimming behavior influences the dispersal of simulated oyster larvae in a coupled particle-tracking

and hydrodynamic model of Chesapeake Bay. Mar. Ecol. Prog. Ser. **359**: 99–115. doi:10.3354/meps07317.

Plummer, M. 2003. JAGS: a program for analysis of Bayesian graphical models using Gibbs sampling. Proceedings of the 3rd International Workshop on Distributed Statistical Computing, Vienna, Austria.

Polansky, L., L. Mitchell, and K. Newman. 2019. Using multistage design-based methods to construct abundance indices and uncertainty measures for Delta Smelt. Trans. Am. Fish. Soc. **148**(4): 710–724. doi: 10.1002/tafs.10166.

Rochette, S., O. Le Pape, J. Vigneau, and E. Rivot. 2013. A hierarchical Bayesian model for embedding larval drift and habitat models in integrated life cycles for exploited fish. Eco. Apps. **23**(7): 1659–1676.

Rose, K.A., Kimmerer, W.J., Edwards, K.P., and Bennett, W.A. 2013. Individual-based modeling of Delta Smelt population dynamics in the upper San Francisco Estuary: II. Alternative baselines and good versus bad years. Trans. Am. Fish. Soc. **142**(5): 1260–1272. doi: 10.1080/00028487.2013.799519.

Royle, J.A. 2004. N-mixture models for estimating population size from spatially replicated counts. Biometrics **60**(1): 108–115.

Simonis, J.L. and Merz, J.E. 2019. Prey availability, environmental constraints, and aggregation dictate population distribution of an imperiled fish. Ecosphere **10**(3): e02634.

Sridharan, V.K., Monismith, S.G., Fong, D.A. and Hench, J.L. 2018. One-Dimensional Particle Tracking with Streamline Preserving Junctions for Flows in Channel Networks. J. Hydraul. Eng. **144**(2).

Smith, W. 2019. Integration of transport, survival, and sampling efficiency in a model of South Delta entrainment. San Francisco Estuary and Watershed Sci (in press).

Sutphin, Z.A. and Svoboda, C.D. 2016. Effects of Hydraulic Conditions on Salvage Efficiency of Adult delta smelt at the Tracy Fish Collection Facility. Tracy Series 43. Available from United States Department of the Interior, Bureau of Reclamation, Washington, D.C. Available from: https://www.usbr.gov/mp//TFFIP/technical-reports.html.

Swanson, C., Young, P.S., and Cech, J.J. 1998. Swimming performance of delta smelt: maximum performance, and behavioral and kinematic limitations on swimming at submaximal velocities. J. Exp. Biol. **201**: 333–345.

Thorson, J.T., Johnson, K.F., Methot, R.D., and Taylor, I.G. 2017. Model-based estimates of effective sample size in stock assessment models using the Dirichlet-multinomial distribution. Fish. Res. **192**: 84–93.

United States Fish and Wildlife Service (USFWS). 2008. Biological opinion on the long-term operational criteria and plan for coordination of the Central Valley Project and State Water Project. Available from: https://www.fws.gov/sfbaydelta/CVP-SWP/index.htm

United States Fish and Wildlife Service (USFWS). 2018. Enhanced delta smelt monitoring 2018 phase 3 sampling preliminary analysis. Available from: https://www.fws.gov/lodi/juvenile_fish_monitoring_program/jfmp_index.htm

Wei, D. 2005. Beijing water resources and the south to north water diversion project. Can. J. Civ. Eng 32: 159–163. doi: 10.1139/l04-113.

White, J.W., Nickols, K.J., Clarke, L., and Largier, J.L. 2010. Larval entrainment in cooling water intakes: spatially explicit models reveal effects on benthic metapopulations and shortcomings of traditional assessments. Can. J. Fish. Aquat. Sci. **67**(12): 2014–2031. doi: 10.1139/F10-108.

Table 1. List of parameter indices, state dynamics probabilities and corresponding model parameters.

Index	Values	Description
f	f = 1, 2 (SWP, CVP)	fish facility
q	q = 1, 2, 3 (Prisoners Point, Lower OMR, Upper OMR)	source region
t	t = 1, 2, 3, … 21 (1995 … 2016)	year
v	v = 1, 2, 3 (April, May, June)	month
s	s = 1, 2, 3, 4 (SWP, CVP, LRZ, IRZ)	sink
l	l = 1, 2, 3, 4, 5	length class

Process	State dynamic probability	Parameters	Parameter description
1. Transport (TR)	$p_{\mathrm{TR_{qtvs}}}$	$n_{\mathrm{S_{tv}}}$	number passing downstream edge of source region,
		$n_{\mathrm{E_{tv}}}$	number entrained
		$\alpha_{\mathrm{TR_{qtvs}}}$, $A_{\mathrm{TR_{qvs}}}$, σ_{TR}	Dirichlet concentration (α), linear regression parameters (A), and standard deviation (σ) of regression parameters for transport
2. Survival (SV)	$p_{\mathrm{SV1_{qtv}}}$		survival of transport to SWP and CVP
	$p_{\mathrm{SV2_{tvs}}}$	β, σ_{SV}	logistic regression parameters for survival across Clifton Court Forebay to State Water Project (SWP), standard deviation of survival
3. Population length structure (LN)	$p_{\mathrm{LN_{tvl}}}$	$\alpha_{\mathrm{LN_{v,}}l}$	Dirichlet concentration for monthly mean population proportion at length
4. Sampling efficiency (EF)	$p_{\mathrm{EF_{tvfl}}}$	Γ_{f}, γ_{ftv}, σ_{EF}	maximum sampling efficiency (Γ), dynamic efficiency (γ), and standard deviation (σ) of dynamic efficiencies
		$p_{\mathrm{BYP_{tvl}}}$, where $p_{\mathrm{BYP_{tvl}}} = f(p_{\mathrm{SEL_{tvl}}}\|\eta_1, l)$	length-based louver selectivity and logistic regression parameters (η)
5. Subsampling		ρ_{tvf}, ω_{tv}	subsampling rate , proportion age-1 fish in fish facility counts

Table 2. Results of the first simulation, testing the estimability of the number of fish entering the source subregion n_S, given assumed transport rates p_{TR} and observed counts at the State Water Project (SWP) and Central Valley Project (CVP). Mean estimated n_S is shown, with associated coefficient of variation in parentheses.

	$n_S = 500$		$n_S = 1{,}000$	
	$p_{TR_{SWP}} = 0.1$	$p_{TR_{SWP}} = 0.4$	$p_{TR_{SWP}} = 0.1$	$p_{TR_{SWP}} = 0.4$
$p_{TR_{CVP}} = 0.05$	498.2 (10.7)	489.2 (4.9)	999.9 (7.5)	999.3 (3.5)
$p_{TR_{CVP}} = 0.3$	499.7 (5.6)	498.8 (2.9)	997.5 (3.8)	999.5 (2.1)

Table 3. Comparison of observed and nominal coverage probabilities for selected parameters, among 500 simulations. α_{TR} and A_{TR} represented transport parameters (Eq. B2-B3), A_{LN} represented population length parameters (Eq. B7), β represented survival parameters (Eq. B6), Γ represented efficiency parameters (Eq. B12), η represented louver selectivity parameters (η_1; Eq. B11), and n_{E} represented the abundance of entrained fish (Eq. 2).

Parameter	95% coverage		Quantiles of z-scores (0.025, 0.975)	
	PTM = p_{TR}	PTM = $p_{\mathrm{TR}} + error$	PTM = p_{TR}	PTM = $p_{\mathrm{TR}} + error$
$\alpha_{\mathrm{TR_{SWP}}}$ and $\alpha_{\mathrm{TR_{CVP}}}$	0.96	0.89	(-3.07, 1.03)	(-4.66, 1.08)
$A_{\mathrm{TR_0}}$	0.96	0.84	(-1.85, 1.95)	(-3.30, 1.77)
$A_{\mathrm{TR_1}}$	0.94	0.90	(-1.99, 2.19)	(-2.19, 2.62)
A_{LN}	0.96	0.96	(-2.32, 0.77)	(-2.22, 0.77)
β_0	0.95	0.94	(-2.21, 1.71)	(-2.34, 1.60)
β_1	0.95	0.95	(-2.09, 1.75)	(-1.90, 1.90)
Γ	0.95	0.94	(-2.03, 1.84)	(-2.10, 1.86)
η	0.94	0.96	(-1.78, 2.19)	(-1.79, 2.11)
n_{E}	0.94	0.94	(-2.40, 1.59)	(-2.41, 1.61)
σ_{TR}	0.97	0.97	(-2.64, 0.91)	(-2.51, 0.95)
σ_{SV}	0.99	0.98	(-1.95, 1.26)	(-2.23, 1.31)
σ_{EF}	0.95	0.95	(-2.42, 1.69)	(-2.27, 1.65)

Table 4. Estimated total entrainment of postlarval delta smelt. Standard deviations of estimates are listed in parentheses.

Year	April	May	June
1995	335 (773)	33 (94)	111 (125)
1996	3,630 (3,394)	198,095 (132,275)	42,523 (26,211)
1997	19,418 (16,076)	201,537 (119,769)	42,246 (20,238)
1998	360 (654)	117 (287)	526 (1,073)
1999	18,047 (13,694)	304,947 (169,533)	501,292 (260,490)
2000	21,469 (17,439)	312,135 (151,684)	168,847 (137,927)
2001	50,333 (35,347)	261,005 (144,519)	146,483 (108,439)
2002	4,765 (3,907)	561,791 (246,423)	60,037 (32,188)
2003	5,037 (4,066)	176,258 (88,236)	45,909 (26,479)
2004	4,608 (5,165)	79,926 (42,366)	36,725 (14,776)
2005	1,672 (1,881)	7,495 (8,248)	5,628 (4,568)
2006	1,235 (1,608)	10 (23)	341 (393)
2007	783 (771)	9,244 (4,970)	10,477 (4,135)
2008	2,929 (3,163)	6,689 (4,271)	5,446 (3,131)
2009	1,202 (1,295)	6,701 (5,720)	6,170 (3,163)
2010	744 (927)	1,035 (1,005)	200 (205)
2011	296 (753)	3,753 (4,927)	1,002 (859)
2012	13,100 (7,717)	32,519 (17,604)	8,899 (4,748)
2013	8,058 (6,467)	28,474 (25,501)	483 (387)
2014	1,072 (1,354)	3,275 (4,303)	32 (35)
2015	3,881 (4,317)	1,877 (2,745)	24 (28)

Table 5. Bayesian P-values for each data component, indicating goodness of fit. P-values represent the proportion of posterior samples in which the model fit observed data better than replicated data, where fit was quantified using the Freeman-Tukey statistic. Particle tracking sinks and fish facilities were the State Water Project (SWP), Central Valley Project (CVP), Low Risk Zone (LRZ) and Indirect Risk Zone (IRZ). Values near 0.5 represent a good fit, with better fit to observed data in exactly half of posterior samples, and values near 0 or 1 indicate poor fit or inability of the model to reproduce observed data.

	Particle tracking				
	SWP	CVP	LRZ	IRZ	
April	0.59	0.58	0.67	0.71	
May	0.63	0.61	0.61	0.55	
June	0.57	0.55	0.51	0.49	
	20mm length composition				
	20-24mm	25-29mm	30-34mm	35-39mm	40-44mm
April	0.82	0.86	0.98	0.98	0.96
May	0.58	0.45	0.47	0.61	0.76
June	0.58	0.57	0.44	0.44	0.66
	Length composition at fish facilities				
April	0.56	0.82	0.73	0.76	0.78
May	0.50	0.41	0.74	0.50	0.35
June	0.58	0.75	0.68	0.71	0.90
	Counts at fish facilities				
	SWP	CVP			
April	0.82	0.68			
May	0.69	0.59			
June	0.66	0.69			

Table 6. Mean relative changes in posterior means of n_E (and the relative change in coefficient of variation) from a sensitivity analysis, showing change due to number of particles used (N_{PT}) in the multinomial model of transport data, reduction of source regions to just the region closest to the water diversions, the survival of postlarval delta smelt in Clifton Court Forebay (p_{SV2}), the inclusion of a length-based selectivity function (p_{SEL}), and to decreasing (-50%) or increasing (+50%) the maximum value of sampling efficiency (Γ). Proportional change was calculated as the difference in posterior mean from the base model divided by posterior mean from the base model (e.g., if difference in n_E from the base model = 50, and the posterior mean of n_E from the base model = 100, then proportional change = 0.5)

Sensitivity analysis	Month		
	April	May	June
N_{PT} = 4,000	-0.18 (-0.02)	-0.22 (-0.03)	0.24 (-0.07)
source region = Upper Old and Middle River	0.01 (-0.04)	0.08 (-0.03)	0.07 (0.01)
p_{SV2} = 1	-0.63 (-0.02)	-0.45 (0.11)	-0.15 (0.01)
p_{SEL} = 1	-0.0004 (-0.01)	0.02 (0.01)	0.01 (0.01)
- 50% Γ	0.42 (-0.01)	0.58 (-0.04)	0.42 (0.05)
+ 50% Γ	-0.31 (0.02)	-0.32 (0.01)	-0.21 (-0.06)

Figure captions

Fig. 1. Map of the west coast of North America, showing the location of the Sacramento-San Joaquin Delta (panel A) and the three subregions of the Sacramento-San Joaquin Delta used in DSM2 particle tracking. The natural direction of net Delta flow is indicated by the open arrows in panel A, but under high water export and low inflow conditions, the direction of flow in the southern portion of the Delta reverses and flows southwards, along the Old and Middle rivers to the pumps. Source subregions are indicated in red (panels B, C and D), and the corresponding Indirect Risk Zone is indicated in yellow but also includes the source subregions. All unshaded areas in the Delta were considered the Low Risk Zone.

Fig. 2. Diagram of the links between the conceptual model of state dynamics, the quantitative model, and data.

Fig. 3. Posterior means from the hierarchical model versus true simulated parameter values.

Fig. 4. Z-scores versus posterior contractions for all model parameters estimated from simulated data.

Fig. 5. Boxplots of posterior distributions of the total numbers of postlarval delta smelt entrained n_{E} in each year. Medians are indicated by the bolded line; interquartile ranges are indicated by the boxes, and the 95% credible interval is indicated by the dashed whiskers.

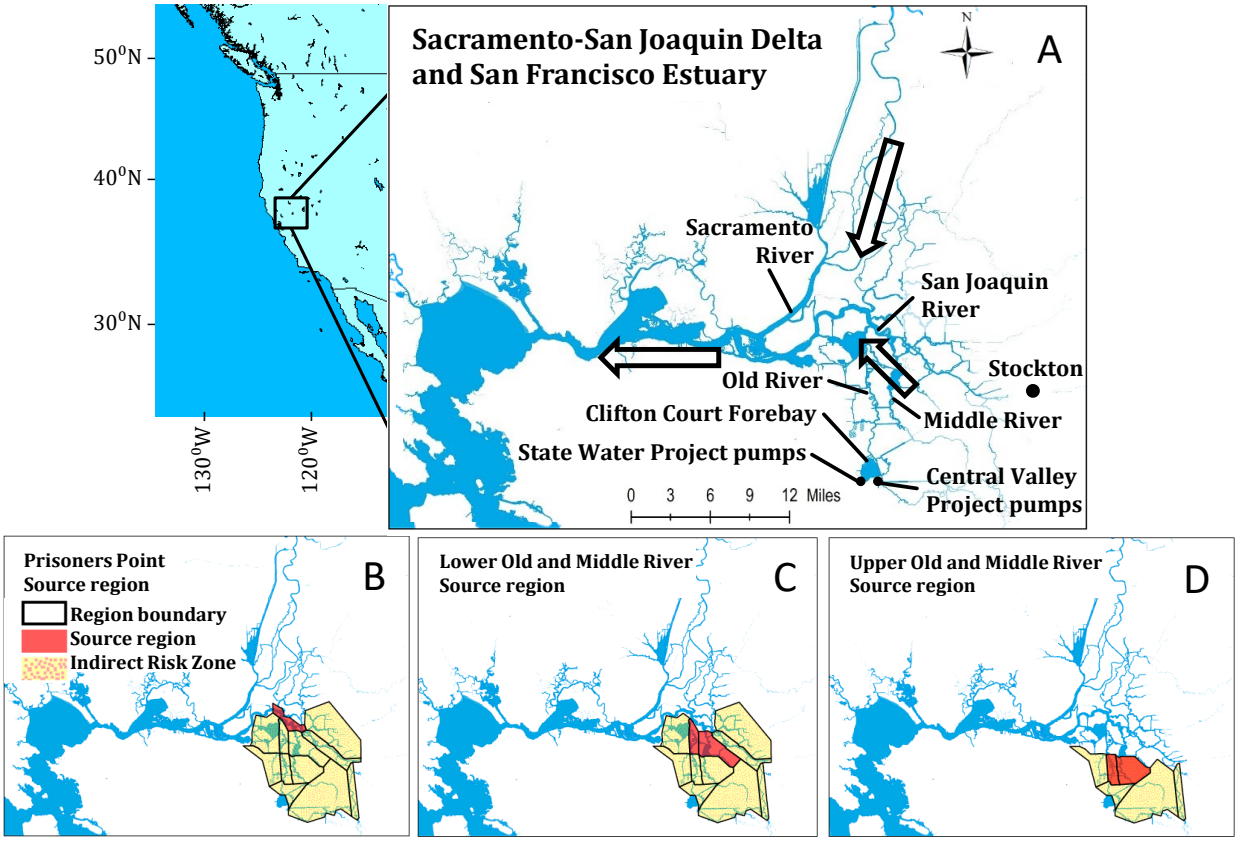
50°N
40°N
30°N
130°W
120°W
Sacramento-San Joaquin Delta and San Francisco Estuary
A
N
Sacramento River
San Joaquin River
Stockton
Old River
Middle River
Clifton Court Forebay
State Water Project pumps
Central Valley Project pumps
0 3 6 9 12 Miles
Prisoners Point Source region
B
Region boundary
Source region
Indirect Risk Zone
Lower Old and Middle River Source region
C
Upper Old and Middle River Source region
D

Figure 1.

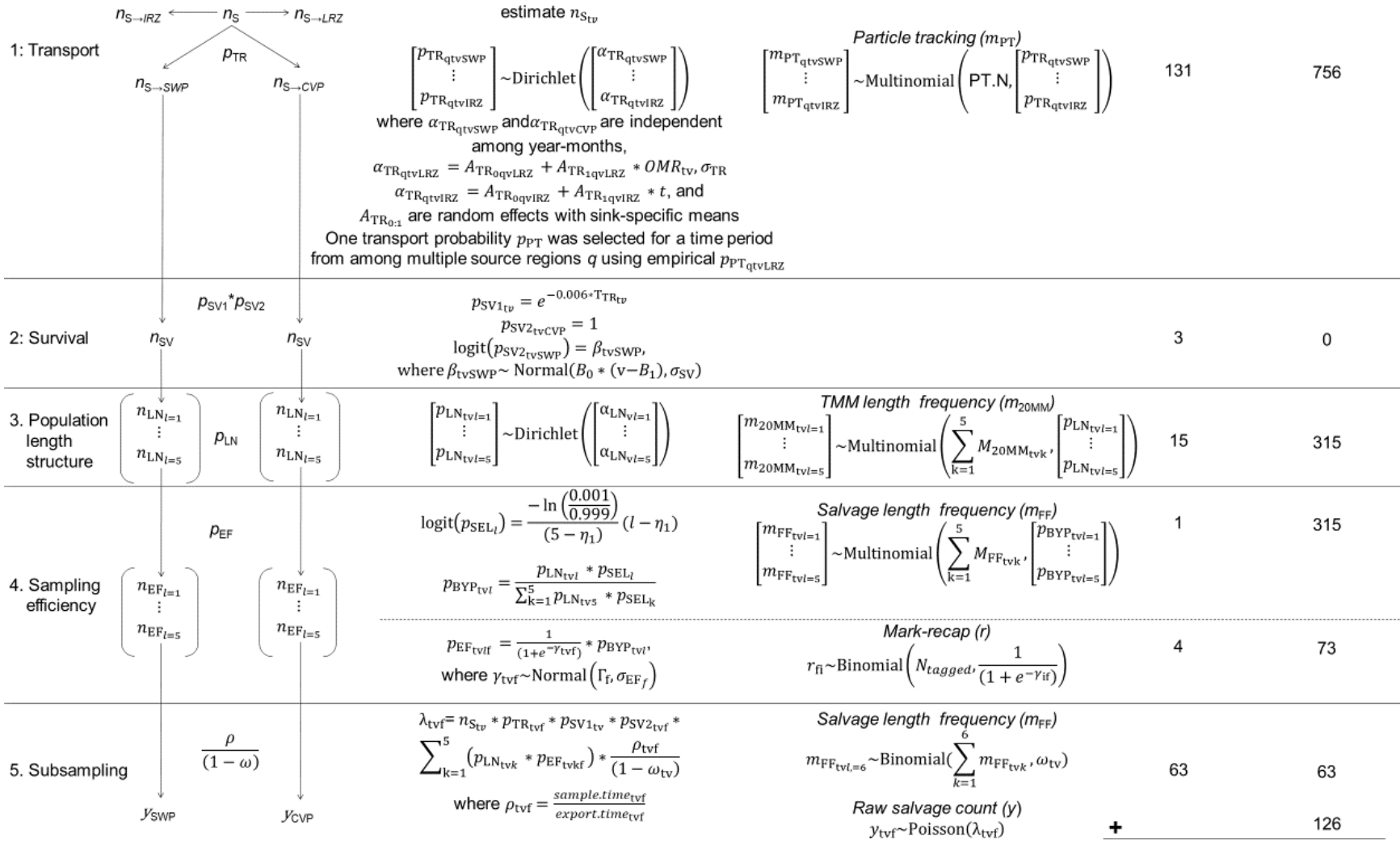
Process
States
State Model
Data
n parameters
n observations
1: Transport
estimate $n_{S_{tv}}$
Particle tracking (m_{PT})
131
756
where $\alpha_{TR_{qtvSWP}}$ and $\alpha_{TR_{qtvCVP}}$ are independent among year-months,
One transport probability p_{PT} was selected for a time period from among multiple source regions q using empirical $p_{PT_{qtvLRZ}}$
2: Survival
3
0
3. Population length structure
TMM length frequency (m_{20MM})
15
315
4. Sampling efficiency
Salvage length frequency (m_{FF})
1
315
Mark-recap (r)
4
73
5. Subsampling
Salvage length frequency (m_{FF})
63
63
Raw salvage count (y)
126
217
1,722

Figure 2.

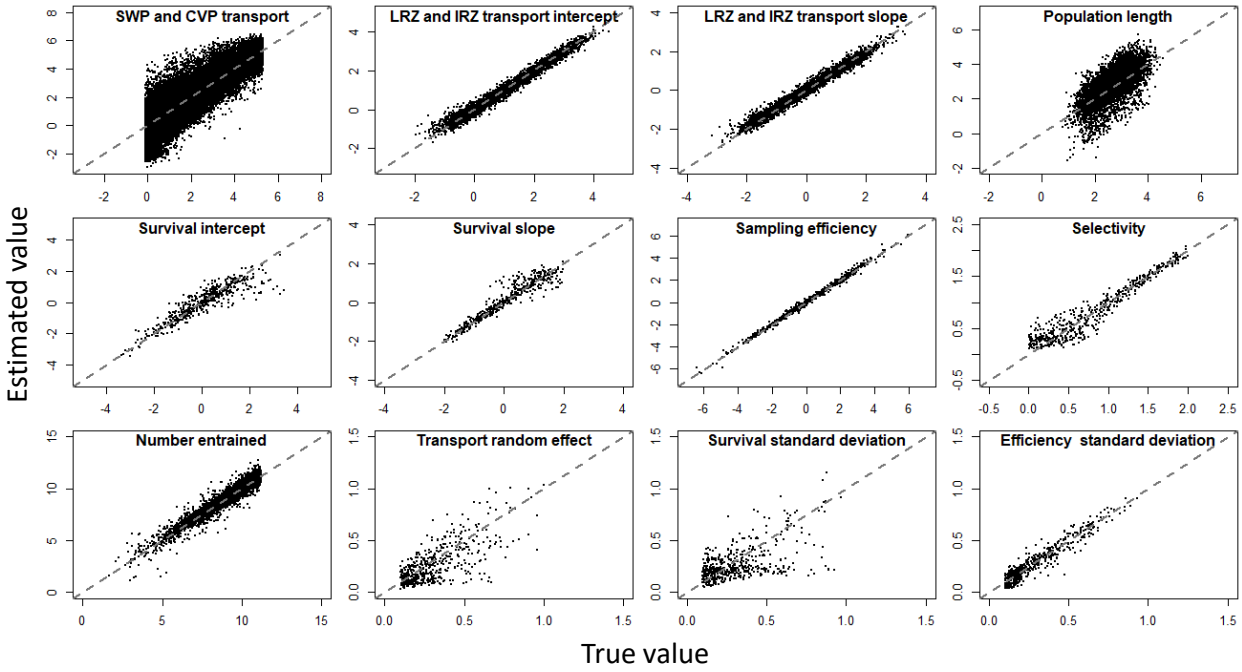

Figure 3.

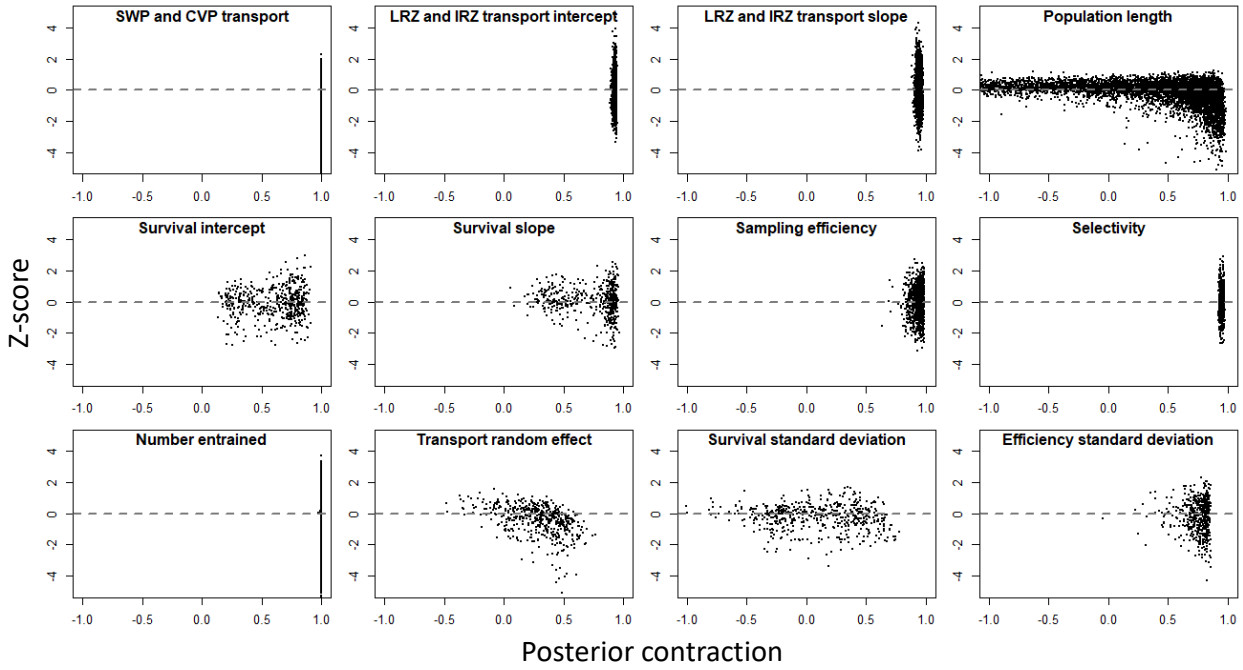

Figure 4.

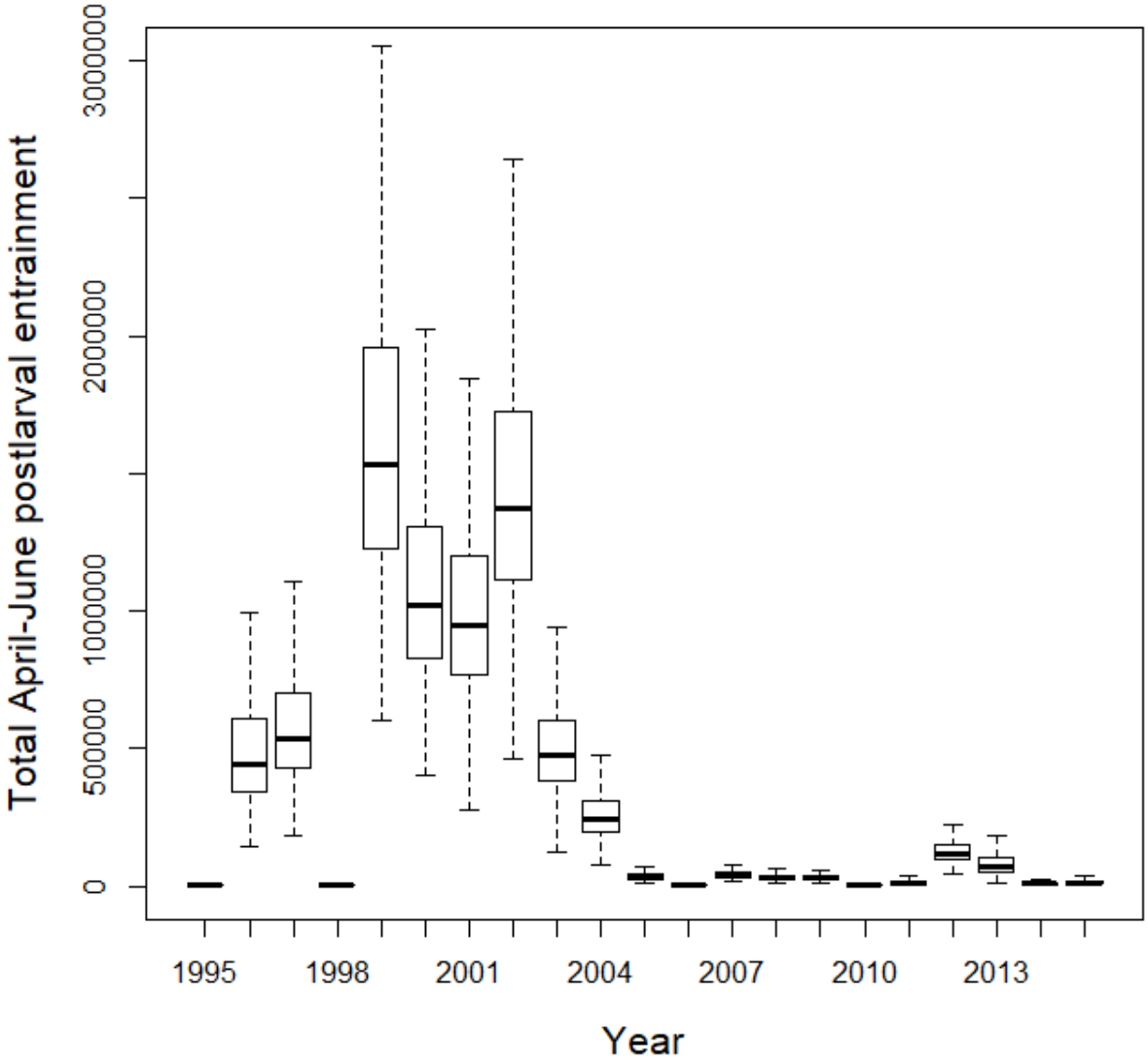
Total April-June postlarval entrainment
0
500000
1000000
2000000
3000000
1995
1998
2001
2004
2007
2010
2013
Year

Figure 5.

Appendix A

Table A1. Particle tracking data, for the Prisoners Point insertion region, informing sub-process 1 (Transport). Data are represented here as proportions reaching each sink ($\frac{m_{PT}}{N_{PT}}$) from the Prisoners Point insertion region. Proportions are organized by year (rows), month (column subheading) and sink (column main heading).

	State Water Project			Central Valley Project			Low Risk Zone			Indirect Risk Zone		
	April	May	June	April	May	June	April	May	June	April	May	June
1995	0.042	0.323	0.333	0.055	0.222	0.210	0.835	0.364	0.315	0.068	0.091	0.142
1996	0.001	0.000	0.096	0.000	0.000	0.056	0.992	0.972	0.797	0.114	0.050	0.050
1997	0.329	0.079	0.007	0.279	0.352	0.369	0.284	0.394	0.418	0.136	0.071	0.100
1998	0.000	0.000	0.002	0.000	0.000	0.003	1.000	0.999	0.938	0.000	0.000	0.000
1999	0.000	0.000	0.000	0.000	0.000	0.000	1.000	1.000	1.000	0.100	0.036	0.021
2000	0.265	0.307	0.303	0.181	0.217	0.202	0.467	0.375	0.388	0.107	0.079	0.100
2001	0.278	0.307	0.338	0.285	0.249	0.267	0.344	0.330	0.262	0.307	0.164	0.257
2002	0.000	0.043	0.115	0.000	0.012	0.062	1.000	0.904	0.732	0.271	0.214	0.171
2003	0.219	0.222	0.223	0.296	0.268	0.283	0.347	0.311	0.323	0.186	0.114	0.043
2004	0.369	0.456	0.265	0.278	0.258	0.286	0.295	0.174	0.294	0.186	0.164	0.007
2005	0.572	0.303	0.226	0.282	0.191	0.296	0.107	0.362	0.323	0.171	0.000	0.029
2006	0.505	0.005	0.012	0.335	0.185	0.330	0.112	0.522	0.387	0.000	0.000	0.071
2007	0.516	0.066	0.043	0.293	0.138	0.079	0.104	0.441	0.516	0.214	0.157	0.007
2008	0.029	0.014	0.036	0.117	0.077	0.069	0.406	0.494	0.541	0.393	0.021	0.121
2009	0.164	0.019	0.108	0.105	0.016	0.078	0.650	0.895	0.705	0.436	0.171	0.157
2010	0.001	0.014	0.003	0.032	0.024	0.099	0.570	0.634	0.497	0.114	0.179	0.107
2011	0.000	0.000	0.001	0.000	0.000	0.000	1.000	1.000	0.998	0.000	0.000	0.014
2012	0.015	0.004	0.399	0.006	0.001	0.242	0.949	0.982	0.308	0.121	0.236	0.257
2013	0.155	0.039	0.178	0.233	0.047	0.349	0.474	0.775	0.371	0.336	0.393	0.300
2014	0.000	0.000	0.000	0.000	0.000	0.000	1.000	1.000	0.999	0.307	0.471	0.007
2015	0.089	0.003	0.038	0.022	0.006	0.146	0.792	0.939	0.737	0.536	0.493	0.021

Table A2. Particle tracking data, for the Lower Old and Middle river insertion region, informing sub-process 1 (Transport). Data are represented here as proportions reaching each sink ($\frac{m_{PT}}{N_{PT}}$) from the Lower Old and Middle river insertion region. Proportions are organized by year (rows), month (column subheading) and sink (column main heading).

	State Water Project			Central Valley Project			Low Risk Zone			Indirect Risk Zone		
	April	May	June	April	May	June	April	May	June	April	May	June
1995	0.257	0.496	0.483	0.254	0.376	0.353	0.433	0.122	0.157	0.057	0.007	0.007
1996	0.008	0.001	0.430	0.015	0.001	0.177	0.813	0.775	0.369	0.114	0.050	0.050
1997	0.608	0.312	0.033	0.251	0.501	0.616	0.123	0.173	0.321	0.136	0.071	0.100
1998	0.162	0.000	0.067	0.000	0.000	0.085	0.825	0.983	0.680	0.000	0.000	0.000
1999	0.000	0.000	0.000	0.000	0.000	0.000	1.000	1.000	1.000	0.100	0.036	0.021
2000	0.504	0.457	0.452	0.373	0.411	0.339	0.115	0.127	0.196	0.107	0.079	0.100
2001	0.510	0.538	0.448	0.390	0.303	0.364	0.092	0.147	0.177	0.307	0.164	0.257
2002	0.000	0.375	0.492	0.000	0.075	0.193	0.998	0.488	0.288	0.271	0.214	0.171
2003	0.411	0.406	0.271	0.476	0.410	0.454	0.103	0.168	0.260	0.186	0.114	0.043
2004	0.486	0.554	0.392	0.424	0.344	0.408	0.086	0.094	0.183	0.186	0.164	0.007
2005	0.642	0.401	0.367	0.310	0.356	0.422	0.046	0.221	0.196	0.171	0.000	0.029
2006	0.588	0.040	0.033	0.356	0.550	0.677	0.053	0.318	0.257	0.000	0.000	0.071
2007	0.635	0.348	0.189	0.319	0.292	0.284	0.042	0.288	0.439	0.214	0.157	0.007
2008	0.331	0.137	0.212	0.506	0.303	0.177	0.114	0.461	0.490	0.393	0.021	0.121
2009	0.518	0.124	0.443	0.341	0.087	0.238	0.119	0.616	0.278	0.436	0.171	0.157
2010	0.022	0.126	0.035	0.305	0.250	0.334	0.466	0.436	0.503	0.114	0.179	0.107
2011	0.000	0.000	0.026	0.000	0.000	0.023	0.997	0.997	0.905	0.000	0.000	0.014
2012	0.252	0.046	0.611	0.130	0.020	0.294	0.510	0.828	0.092	0.121	0.236	0.257
2013	0.386	0.238	0.266	0.446	0.260	0.573	0.147	0.438	0.154	0.336	0.393	0.300
2014	0.000	0.000	0.000	0.000	0.000	0.000	1.000	0.987	0.977	0.307	0.471	0.007
2015	0.613	0.053	0.130	0.113	0.063	0.520	0.203	0.648	0.326	0.536	0.493	0.021

Table A3. Particle tracking data, for the Upper Old and Middle river insertion region, informing sub-process 1 (Transport). Data are represented here as proportions reaching each sink ($\frac{m_{PT}}{N_{PT}}$) from the Upper Old and Middle river insertion region. Proportions are organized by year (rows), month (column subheading) and sink (column main heading).

	State Water Project			Central Valley Project			Low Risk Zone			Indirect Risk Zone		
	April	May	June	April	May	June	April	May	June	April	May	June
1995	0.381	0.507	0.570	0.363	0.445	0.351	0.250	0.048	0.080	0.007	0.000	0.000
1996	0.085	0.036	0.671	0.077	0.012	0.181	0.752	0.832	0.147	0.114	0.050	0.050
1997	0.886	0.569	0.103	0.070	0.368	0.682	0.041	0.063	0.215	0.136	0.071	0.100
1998	0.908	0.000	0.577	0.034	0.000	0.194	0.058	0.999	0.223	0.000	0.000	0.000
1999	0.000	0.000	0.000	0.000	0.000	0.000	1.000	1.000	1.000	0.100	0.036	0.021
2000	0.543	0.567	0.493	0.427	0.377	0.408	0.028	0.056	0.098	0.107	0.079	0.100
2001	0.525	0.510	0.475	0.450	0.421	0.438	0.023	0.069	0.087	0.307	0.164	0.257
2002	0.000	0.786	0.629	0.000	0.067	0.279	1.000	0.142	0.091	0.271	0.214	0.171
2003	0.447	0.515	0.353	0.514	0.408	0.499	0.038	0.077	0.147	0.186	0.114	0.043
2004	0.423	0.521	0.506	0.556	0.433	0.384	0.019	0.044	0.109	0.186	0.164	0.007
2005	0.670	0.331	0.325	0.318	0.581	0.573	0.012	0.084	0.101	0.171	0.000	0.029
2006	0.638	0.072	0.013	0.349	0.850	0.850	0.014	0.071	0.137	0.000	0.000	0.071
2007	0.694	0.698	0.358	0.297	0.145	0.381	0.010	0.152	0.257	0.214	0.157	0.007
2008	0.625	0.345	0.299	0.357	0.346	0.337	0.017	0.302	0.357	0.393	0.021	0.121
2009	0.587	0.279	0.607	0.396	0.171	0.293	0.014	0.519	0.096	0.436	0.171	0.157
2010	0.049	0.223	0.171	0.803	0.580	0.400	0.134	0.187	0.422	0.114	0.179	0.107
2011	0.000	0.000	0.077	0.000	0.000	0.056	1.000	1.000	0.827	0.000	0.000	0.014
2012	0.607	0.126	0.672	0.279	0.034	0.295	0.109	0.784	0.033	0.121	0.236	0.257
2013	0.379	0.459	0.366	0.564	0.307	0.562	0.053	0.231	0.071	0.336	0.393	0.300
2014	0.000	0.000	0.000	0.000	0.000	0.000	1.000	1.000	1.000	0.307	0.471	0.007
2015	0.857	0.337	0.174	0.097	0.153	0.648	0.038	0.479	0.177	0.536	0.493	0.021

Table A4. Mark-recapture data reported by Castillo et al. (2012) and used to model maximum sampling efficiency (Eq. B13) at the Skinner Fish Facility. N_{EF} delta smelt were tagged and released in each trial (rows), and r were recovered.

N_{EF}	r
100	39
100	36
100	89
100	49
100	43
100	45

Table A5. Mark-recapture data reported by Sutphin and Svoboda (2016) and used to model maximum sampling efficiency (Eq. B13) at the Tracy Fish Facility. N_{EF} delta smelt were tagged and released in each trial (rows), and r were recovered.

N_{EF}	r	N_{EF}	r	N_{EF}	r
180	20	100	35	75	31
179	21	100	28	75	31
179	52	100	35	130	38
179	55	100	11	130	70
180	27	100	6	130	56
180	29	100	23	130	72
176	19	75	39	130	36
178	27	75	28	130	17
180	16	75	29	130	14
180	23	75	25	130	36
400	124	75	24	130	0
80	26	75	28	130	0
80	21	75	24	130	1
80	13	75	26	100	0
80	38	75	28	100	1
80	12	75	27	100	0
78	8	75	24	100	5
76	9	75	28	100	3
80	13	75	17	100	4
80	5	75	27	100	18
80	7	75	19	100	10
80	4	75	45	100	16
79	10				

Appendix B

Mathematical model

Sub-process 1: Transport of fish to facilities. We modeled transport probabilities $p_{\mathrm{TR}_{qtvs}}$ from source region q (Fig. 1) to sink s in year t and month v (Table 1) using a Dirichlet distribution with parameters $\alpha_{\mathrm{TR}_{qtvs}}$. Hereafter, we denote vectors in bold and the full set of an indexed value with a period. For s in the set (1, 2, 3, 4 [State Water Project {SWP}, Central Valley Project {CVP}, Low Risk Zone {LRZ}, Intermediate Risk Zone {IRZ}]), let the vector

(B1) $$\mathbf{p}_{\mathrm{TR}_{qtv.}} \sim \mathrm{Dirichlet}(\boldsymbol{\alpha}_{\mathrm{TR}_{qtv.}}).$$

Both particle tracking data and fish facility fish count data were available to inform time-specific estimates of the parameters $\alpha_{\mathrm{TR}_{qtv1}}$ and $\alpha_{\mathrm{TR}_{qtv2}}$ (SWP and CVP); however, $\alpha_{\mathrm{TR}_{qtv3}}$ and $\alpha_{\mathrm{TR}_{qtv4}}$ (LRZ and IRZ) were informed by particle tracking data only. Hence, transport to LRZ (s=3) was modeled as a log-linear function of hydrodynamic covariate *OMR* and month-specific linear regression parameters A_{TR}

(B2) $$\log(\alpha_{\mathrm{TR}_{qtv3}}) = A_{\mathrm{TR}_{0qv3}} + A_{\mathrm{TR}_{1qv3}} OMR_{\mathrm{tv}},$$

and transport to IRZ (s=4) was modeled as a log-linear function of year,

(B3) $$\log(\alpha_{\mathrm{TR}_{qtv4}}) = A_{\mathrm{TR}_{0qv4}} + A_{\mathrm{TR}_{1qv4}} t.$$

Intercept and slope A_{TR} were assumed to be similar among months and source regions, for the same sink; therefore, all intercept and slope A_{TR} were modeled as normally distributed random effects of a single sink-specific intercept and slope.

Let $\mathrm{m}_{\mathrm{PT}_{\mathrm{qtvs}}}$ represent the number of particles in the particle tracking model that were released in source region q in year t and month v that reached sink s by the end of the month. We assumed these counts followed a multinomial distribution with total effective number of particles N_{PT} and probability vector

$$\mathbf{p}_{\mathrm{TR}_{\mathrm{qtv}\cdot}}$$

$$\text{(B4)} \qquad \mathbf{m}_{\mathrm{PT}_{\mathrm{qtv}\cdot}} \sim \mathrm{Multinomial}\left(N_{\mathrm{PT}}, \mathbf{p}_{\mathrm{TR}_{\mathrm{qtv}\cdot}}\right).$$

The number of particles released in a source region in the particle tracking model (4,000) was an arbitrarily large number. As multinomial variance scales with sample size, the effect of particle tracking data on parameter estimates could be made arbitrarily large. To remove this arbitrary consequence, we derived a single effective multinomial sample size N_{PT} using the method described by McAllister and Ianelli (1997).

Sub-process 2: Survival. Using OMR flow divided by mean Old and Middle River cross sectional area between the mouths of Old and Middle rivers and the SWP and CVP, as an estimate of mean monthly water velocity, and the distance between the midpoint of each source region and the SWP and CVP, year-month-source specific transport times (days) $T_{\mathrm{TR}_{\mathrm{qtv}}}$ were calculated as distance divided by velocity. Zero or downstream OMR flow resulted in infinite transport time using this method, so T_{TR} was truncated at 15 days to represent mortality at the midpoint of one month. Daily mortality of 0.006 was estimated for larval through subadult lifestages of delta smelt by Bennett (2005) using daily otolith ages and catch

curve analysis. To develop survival probabilities for each year-month combination, transport times were multiplied by the Bennett (2005) daily mortality rate and converted to survival rates $p_{\mathrm{SV1}_{\mathrm{qtv}}}$ (Fig. D1)

(B5) $$p_{\mathrm{SV1}_{\mathrm{qtv}}} = e^{-0.006T_{\mathrm{TR}_{\mathrm{qtv}}}}.$$

$p_{\mathrm{SV1}_{\mathrm{qtv}}}$ for the source region selected as the source for a year-month was applied to all fish arriving at the SWP and CVP.

The probability of a delta smelt surviving the journey from the Forebay radial gates (where the forebay connects to Old River) to the SWP intake channel in a given year and month $p_{\mathrm{SV2}_{\mathrm{tv1}}}$ was treated as a logit-normal random variable:

(B6) $$\mathrm{logit}(p_{\mathrm{SV2}_{\mathrm{tv1}}}) \sim \mathrm{Normal}(\beta_0 + \beta_1 v, \sigma_{\mathrm{SV2}});$$

thus, the survival probability increased or decreased with time (and age). CVP does not have a forebay, so set $p_{\mathrm{SV2}_{\mathrm{tv2}}}$ was set to 1.

Sub-process 3: Population length structure. Let $p_{LN_{\mathrm{tvl}}}$ represent the population length frequency for length class *l*. We modeled these quantities using a Dirichlet random variable with month-length specific parameters $\alpha_{LN_{\mathrm{vl}}}$. For *l* in the set (1, 2, … 5), let the vector

(B7) $$\mathbf{p}_{\mathrm{LN}_{\mathrm{tv}\cdot}} \sim \mathrm{Dirichlet}(\boldsymbol{\alpha}_{\mathrm{LN}_{\mathrm{v}\cdot}}).$$

By using this structure, we assumed that length distributions within the same month were similar across years.

We modeled the vector of adjusted counts $\mathbf{m}_{20\text{MM}_{\text{tv}\cdot}}$ with a multinomial distribution

(B8) $$\mathbf{m}_{20\text{MM}_{\text{tv}\cdot}} \sim \text{Multinomial}\left(N_{20\text{MM}_{\text{tv}}}, \mathbf{p}_{\text{LN}_{\text{tv}\cdot}}\right).$$

We adjusted the length data from the 20mm Survey to account for gear selectivity (Mitchell et al. 2019). Gear selectivity uncertainty was found to be a relatively minor source of variability in 20mm Survey data compared to other sources of variability (Polansky et al. 2019), so it was ignored for this analysis. We made these adjustments by dividing observed delta smelt counts in each of the five length bins by estimates of 20mm Survey gear selectivity at the midpoints of each bin (and rounding to the nearest integer value), resulting in estimates of the number of fish that would have been caught if the gear could catch all available fish with 100% efficiency.

For the effective sample sizes $N_{20\text{MM}_{\text{tv}}}$ we used the total number of tows, conducted by the 20mm Survey in which the length data were collected. We scaled the adjusted counts so they summed to $N_{20\text{MM}_{\text{tv}}}$. Length samples of fish populations may exhibit overdispersion due to the tendency of fish to aggregate by length or age. The standard approach to address this overdispersion when estimating population proportion at length, from multinomially distributed length samples, is to set the effective multinomial sample size to the number of tows (McAllister and Ianelli 1997). Note that this approach was different from the approach used to derive N_{PT}, for which information such as number of tows does not exist.

Sub-process 4: Sampling efficiency at fish facilities. We first estimated selectivity probability-at-length p_{SEL_l} with fish facility length data using a logistic function with an asymptotic maximum value of one. Given that the louvers are similar for the SWP and CVP, we used the same length-based louver selectivity model for both facilities, but estimated facility-specific maximum efficiencies. Let $m_{\text{FF}_{\text{tv}l}}$ represent the

number of delta smelt in length class l that were diverted and measured at fish facilities. We assumed these counts followed a multinomial distribution with effective sample size $N_{\mathrm{FF_{tv}}}$ and probability vector

$$\mathbf{p}_{\mathrm{BYP_{tv\cdot}}}$$

(B9) $$\mathbf{m}_{\mathrm{FF_{tv\cdot}}} \sim \mathrm{Multinomial}\left(N_{\mathrm{FF_{tv}}}, \mathbf{p}_{\mathrm{BYP_{tv\cdot}}}\right).$$

We set the effective sample size $N_{\mathrm{FF_{tv}}}$ equal to the total number of days (in year t and month v) on which fish were counted and measured, summed across the two fish facilities. $m_{\mathrm{FF_{tvl}}}$ were then rescaled to sum to $N_{\mathrm{FF_{tv}}}$. The probabilities $p_{\mathrm{BYP_{tvl}}}$ represent the length frequency distribution of fish diverted to the holding tanks. We calculated these probabilities as the scaled product of the population length structure $p_{\mathrm{LN_{tvl}}}$ and the length-based louver selectivity p_{SEL_l}:

(B10) $$p_{\mathrm{BYP_{tvl}}} = p_{\mathrm{LN_{tvl}}} p_{\mathrm{SEL}_l} \Big/ \sum_{\mathrm{k}=1}^{5} p_{\mathrm{LN_{tvk}}} p_{\mathrm{SEL_k}}.$$

We used a logistic function to describe louver selectivity:

(B11) $$p_{\mathrm{SEL}_l} = 1 \Big/ \left(1 + e^{-\eta_0 (l - \eta_1)}\right),$$

where l takes the values 1, 2, 3, 4, and 5 (representing the five length bins), η_0 controls the steepness of the curve, and η_1 is the l value at which $p_{\mathrm{SEL}_l} = 0.5$. We assumed fish in the fifth length bin had the highest selectivity probability relative to the other bins (i.e., $p_{\mathrm{SEL}_5} = 0.999$), which allowed us to solve for η_0 analytically: $\eta_0 = \frac{-\ln\left(\frac{0.001}{0.999}\right)}{(5 - \eta_1)}(l - \eta_1)$. The parameter η_1, was estimated during model fitting.

We defined the length-specific probabilities of fish being diverted to the fish facilities, or overall sampling efficiency, $p_{\mathrm{EF}_{\mathrm{tvf}l}}$ of fish facility *f* for diverting length-*l* delta smelt as

$$\text{(B12)}\quad p_{\mathrm{EF}_{\mathrm{tvf}l}} = \frac{1}{\left(1 + e^{-\gamma_{\mathrm{ftv}}}\right)} p_{\mathrm{SEL}_l},$$

where the fraction on the right hand side is a facility-specific scaling factor between 0 and 1 and γ were maximum sampling efficiencies. We estimated year-month-facility specific γ_{ftv} using a Bayesian model fit to the mark-recapture experiment data sets. These models were fit externally to the hierarchical model described in this article. Note that γ for mark-recapture experiments were indexed by trial number, but γ for fish facility counts (Eq. 12) were indexed by year and month. Let $N_{\mathrm{EF}_{\mathrm{fi}}}$ be the number of delta smelt tagged in experiment number *i* at fish facility *f* and let r_{fi} be the number of fish recovered in the holding tanks. We assumed r_{fi} followed a binomial distribution,

$$\text{(B13)}\quad r_{\mathrm{fi}} \sim \mathrm{Binomial}\left(N_{\mathrm{EF}_{\mathrm{fi}}}, \frac{1}{\left(1 + \mathrm{e}^{-\gamma_{\mathrm{fi}}}\right)}\right),$$

with $N_{\mathrm{EF}_{\mathrm{fi}}}$ trials and success probability $\frac{1}{\left(1 + e^{-\gamma_{\mathrm{fi}}}\right)}$. Each γ_{fi} (and γ_{ftv} for year-months of entrainment) was normally distributed with facility-specific mean Γ_{f} and standard deviation $\sigma_{\mathrm{EF}_{\mathrm{f}}}$

$$\text{(B14)}\quad \gamma_{\mathrm{fi}} \sim \mathrm{Normal}\left(\Gamma_{\mathrm{f}}, \sigma_{\mathrm{EF}_{\mathrm{f}}}\right).$$

Because adult delta smelt were used in the experiments, we assumed relative size selectivity (i.e., p_{SEL_l}) was one for all tagged fish.

Sub-process 5: Subsampling at fish facilities. We estimated the probability ω_{tv} with count-at-length data from the fish facilities. Using the same five length bins as in the population length structure sub-process, and defining a sixth bin to represent 45+ mm delta smelt, we modeled the number of delta smelt in the sixth bin $m_{\text{FF}_{\text{tv6}}}$ using a binomial distribution:

(B15) $m_{\text{FF}_{\text{tv6}}} \sim \text{Binomial}(\sum_{\text{k}=1}^{6} m_{\text{FF}_{\text{tvk}}}, \omega_{\text{tv}})$.

Number of fish at entrained: We used estimates of postlarval delta smelt abundance from the entire Delta for May and June (Polansky et al. 2019) to develop weakly informative lognormal priors for the number of delta smelt passing through the source region $n_{\text{S}_{\text{tv}}}$ with support, defined as the 99% prior predictive interval, from approximately 0.002 to 4.5 times abundance. Because these abundance estimates were only available for the months of May and June, we set an upper bound for April equal to either the maximum of May abundance or a retrospective extrapolation of May to June abundance. This accounted for periodic years of early recruitment, as evident by declining May to June abundance when April postlarval abundance may have been higher than May.

Simulation model and data

In the first set of simulations, independence was assumed among the individual fish comprising n_{S}, and the numbers ending up in each of the four sinks y_s were a multinomial random vector with probability p_{s}, where s was in the set (1, 2, 3, 4 [SWP, CVP, LRZ, IRZ]). Given that y_3 and y_4 (LRZ and IRZ) were unobserved, the distribution for y_1 and y_2 (SWP and CVP) alone was a simpler multinomial

(B16) $\mathbf{y}. \sim \text{Multinomial}(n_{\text{S}}, \mathbf{p}.)$, where $s \in (1, 2)$.

Given known values for p_1 and p_2, n_S is clearly estimable, e.g., y_1/p_1 is a method of moments estimate. Maximum likelihood estimates (MLEs) of n_S, which are more efficient than the Bayesian hierarchical model, can be calculated by a grid search for n_S over the integer set ($y_1 + y_2$, $y_1 + y_2 + 1$, …). A simulation study was carried out to examine the quality of the MLEs. For each of eight combinations of values of n_S (500 or 1,000), p_1 (0.1 or 0.4), and p_2 (0.05 or 0.30), 1,000 simulations of y_1 and y_2 were generated from the simpler multinomial model and MLEs for n_S were calculated and compared to true values.

A second simulation study examined estimability of key parameters under a much more complex Bayesian hierarchical model that closely paralleled the one applied to the real data and integrated data from multiple sources. The hierarchical model described above was used to define an operating model, based loosely on the parameters estimated for delta smelt. New particle tracking, length composition, and fish facility sample data were stochastically simulated to generate 500 replicate datasets. Each model parameter (n_S, α_{TR}, α_{LN}, β, η, and Γ) was drawn from a uniform distribution to simulate a set of true state dynamics (Eqs. B1, B6, B7, and B13). From the set of true states, observed data were then simulated based on the models for observed values (Eqs. B4, B8, B9, B13, B15, and 1). The estimation model was the same as the operating model; it would therefore fit the simulated data perfectly in the absence of observation error, if all parameters were estimable. The model was then fit to each simulated dataset. The estimability of each parameter was evaluated using three metrics that compared estimated to true values (Betancourt 2018): 95% credible interval coverage of the true value, z-scores indicating deviations between true simulated and estimated values,

$$\text{(B17)} \quad z_{tv} = \left(\text{mean}(\text{true } n_{S_{tv}}) - \text{mean}(\text{estimated } n_{S_{tv}})\right)/\text{sd}(\text{true } n_{S_{tv}}),$$

and posterior contraction comparing the prior to posterior standard deviation

(B18) $contraction_{\mathrm{tv}} = 1 - \mathrm{sd}(\mathrm{posterior}\ n_{\mathrm{S_{tv}}})/\mathrm{sd}(\mathrm{prior}\ n_{\mathrm{S_{tv}}})$.

Additional simulations focused on the effect of errors in the particle tracking model based probabilities of movement from the source region to the four sinks on posterior distributions of key parameters. Particle tracking data were assumed to represent observations of the transport process, with some unknown level of additional noise induced by the disconnect between simulated hydrodynamics and true delta smelt transport rates. To assess model performance with noisy transport information, two sets of simulations were performed, one set in which new particle tracking data were simulated from true transport rates and one set in which particle tracking data were simulated from true transport parameters, times random lognormal error. That is, Eq. 1 was modified to

(B19) $\mathbf{p}_{\mathrm{TR_{qtv.}}} \sim \mathrm{Dirichlet}\left(\boldsymbol{\alpha}_{\mathrm{TR_{qtv.}}} \times e^{\boldsymbol{error}_{\mathrm{tv.}}}\right)$,

where *error* was normally distributed with mean 0 and standard deviation 0.3.

Model fitting and diagnostics

While a weakly informative uniform prior distribution was derived for n_{source}, uninformative priors were used for all other parameters. Dirichlet parameters α were given Gamma(0.01,0.01) priors, and all logistic regression priors β, η, and γ were drawn from Normal(0,$\sqrt{\pi^2/6}$) distributions. A Normal(0,$\sqrt{\pi^2/6}$) distribution induced the desired Uniform(0,1) distribution on inverse logistic transformation. Hyper-parameters for the linear models of LRZ and IRZ transport probability (Eq. C1 and C2) were assigned Normal(0, $\sqrt{20}$) priors. Penalized complexity prior distributions, Exponential(4.6), were assigned to all

standard error parameters σ (Simpson et al. 2017), assuming a prior probability of 0.01 that σ exceeded a value of 1.

The model was fit using R package R2jags (Su and Yajima 2015) and Markov Chain Monte Carlo program JAGS (Plummer 2003). R code to run the model is in Appendix C. A burn-in period of 50,000 was followed by 300,000 samples of posterior distributions among six chains. As preliminary analysis suggested autocorrelation within posterior chains, posterior samples were thinned by 25. Model convergence was assessed by comparing the trace plots of six chains of each model parameter and using Gelman and Rubin's diagnostic (Gelman and Rubin 1992). Model convergence was assumed if trace plots showed that all chains were producing samples of parameters with similar posterior distributions that did not shift with additional samples and if Gelman and Rubin's statistic was less than 1.05 for all parameters. Correlation between parameters was assessed by calculating coefficients of determination (R^2) for all pairwise combinations of parameter posteriors. Residual plots of the fish facility counts, population length structure, and fish facility sampling efficiency models were explored for evidence of model fit and bias.

A graphical posterior predictive check was performed and Bayesian P-values were calculated for each data component (*PT*, m_{20mm}, m_{FF}, and *obs*). Each data component was replicated from the fitted model, and Bayesian P-values were based on a comparison of goodness of fit to replicated and observed data. Replicated and observed goodness of fit were compared using the Freeman-Tukey statistic *FT*, calculated for each observed and replicated data point ($FT = \sum(\sqrt{observed} - \sqrt{expected})^2$; Cressie and Read 1984). *FT* were summed over dimensions reflecting the hierarchical model structure. FT_{PT} and FT_{obs} were summarized for each fish facility-month combination by summing over years. FT_{20mm} and FT_{FF} were summarized for each length-month combination by summing over years. Graphical analyses were performed by comparing $FT_{replicated}$ and $FT_{observed}$ from all 300,000 Monte Carlo simulations, and P-values were calculated as the number of joint posterior samples of *FT* where $FT_{replicated} \geq FT_{observed}$, divided

by the total number of samples. When the model is sufficient to replicate observed data, Bayesian P-values are near 0.5. P-values greater than 0.95 and less than 0.05 demonstrated a low probability that the model can reproduce observed data and were considered an indication of poor model fit.

References

Bennett, W.A. 2005. Critical assessment of the delta smelt population in the San Francisco Estuary, California. San Francisco Estuary Watershed Sci, 3. Available from: https://escholarship.org/uc/item/0725n5vk.

Betancourt, M. 2018. Towards a principled Bayesian workflow. Available from: https://betanalpha.github.io/assets/case_studies/principled_bayesian_workflow.html

Cressie, N., and Read, T.R. 1984. Multinomial goodness-of-fit tests. J. R. Stat. Soc. Series B Stat. Methodol. **46**(3): 440–464.

Gelman, A. and Rubin, D.B. 1992. Inference from iterative simulation using multiple sequences. Stat. Sci. **7**: 457–511.

McAllister, M.K. and Ianelli, J.N. 1997. Bayesian stock assessment using catch-age data and the sampling-importance resampling algorithm. Can. J. Fish. Aquat. Sci. **54**(2): 284–300.

Mitchell, L., Newman, K., and Baxter. R. 2019. Estimating the size selectivity of fishing trawls for short-lived fish species. San Francisco Estuary and Watershed Sci. **17**(1). Available from: https://doi.org/10.15447/sfews.2018v17iss1art5.

Plummer, M. 2003. JAGS: a program for analysis of Bayesian graphical models using Gibbs sampling. Proceedings of the 3rd International Workshop on Distributed Statistical Computing, Vienna, Austria.

Polansky, L., L. Mitchell, and K. Newman. 2019. Using multistage design-based methods to construct abundance indices and uncertainty measures for Delta Smelt. Trans. Am. Fish. Soc. **148**(4): 710–724. doi: 10.1002/tafs.10166.

Simpson, D., Rue, H., Riebler, A., Martins, T.G., and Sørbye, S.H. 2017. Penalising model component complexity: A principled, practical approach to constructing priors. Stat. Sci. **32**: 1–28.

Su, Y.S. and Yajima, M. 2015. R2jags: Using R to Run `JAGS'. Version 0.5-7. https://CRAN.R-project.org/package=R2jags.

Appendix B

JAGS code to fit model

```
### Calculate survival of transport (p.SV1) outside of BHM ###
distance=c(NA,33070,25360,16625)
survival.transport=matrix(NA,Y,M)
days=matrix(NA,Y,M)
for (y in startY:Y) {
  for (v in 1:M) {
  if (OMR[t,v] < 0) {
     #T.TR=distance/flow/area/feet/meter/seconds/day
     T.TR[t,v] <- (distance[PTM.map[t,v]]/(abs(OMR[t,v])/7659.96)/0.3048)/(3600*24)
     p.SV1[t,v] <- max(exp(-0.006*15),exp(-0.006*T.TR[y,v]))
     }
  else {
     p.SV1[t,v] <- exp(-0.006*15)
     }
     }
  }

### JAGS model ###
model {

### Priors ###
# Latent states #
for (t in startY:Y) {
  for (v in 1:M) {
     n.source[t,v] ~ dlnorm(log(0.01*nhat[(t-16),v]),(1/log(10))
     }
  }

# Sub-process 1: Transport #
sigma.TR ~ dexp(4.6)
tau.TR <- pow(sigma.TR,-2)
for (i in 3:4) {
  hyper.A.TR[i,1] ~ dnorm(0,0.05)
  hyper.A.TR[i,2] ~ dnorm(0,0.05)
  }
for (q in 1:3) {
for (v in 1:M) {
  for (t in startY:Y) {
     for (i in 1:2) {
        log.alpha.TR[q,t,v,i] ~ dnorm(0,0.05)
        alpha.TR[q,t,v,i] <- exp(log.alpha.TR[q,t,v,i])
        }
     }
  for (i in 3:4) {
     for (j in 1:2) {
        A.random[q,v,i,j] ~ dnorm(0,tau.TR)
        }
     A.TR[q,v,i,1] <- hyper.A.TR[i,1] + A.random[q,v,i,1]
     A.TR[q,v,i,2] <- hyper.A.TR[i,2] + A.random[q,v,i,2]
     }
  for (t in startY:Y) {
     alpha.TR[q,t,v,3] <- A.TR[q,v,3,1]+A.TR[q,v,3,2]*OMR[t,v]
```

```
      alpha.TR[q,t,v,4] <- A.TR[q,v,4,1]+A.TR[q,v,4,2]* (((t-startY+1)-11)/6.2)
      }
  }

# Sub-process 2: Survival #
beta[1] ~ dnorm(0,0.61)
beta[2] ~ dnorm(0,0.61)

# Sub-process 3: Population length structure #
for (l in 1:5) { # population length structure
  for (v in 1:M) {
      alpha.LN[v,l] ~ dgamma(0.001,0.001)
      }
  }

# Sub-process 4: Sampling efficiency
eta[1] <- -log(0.001/0.999)/(5-eta[2]) # selectivity
eta[2] ~ dnorm(0,0.30)
G[1] <- 0.067 # max efficiency
G[2] <- -1.586
sigma.EF[1] <- 1.102
sigma.EF[2] <- 1.259
for (f in 1:2) {
  tau.EF[f] <- pow(sigma.EF[i],-2)
  }

# Sub-process 5: Subsampling #
for (t in startY:Y) {
  for (v in 1:M) {
      omega[t,v] ~ dunif(0,1)

### Model ###
# Sub-process 1: Transport #
# Data (PT) are organized by t=year, m=month, sink (1:4) #
for (q in 1:3) {
        p.PT[q,t,v,(1:4)] ~ ddirch(alpha.TR[q,t,v,(1:4)])
        m.PT[t,v,(1:4),q] ~ dmulti(p.TR[q,t,v,(1:4)],M.PT)
        }
      p.TR[t,v,(1:4)] <- p.PT[PT.map[t,v],t,v,(1:4)]
      n.entrain[t,v] <- n.edge[t,v]*(1-p.TR[t,v,3])

# Sub-process 2: Survival #
      p.survival[t,v,1] <- p.SV1[t,v]*ilogit(beta[1]+beta[2]*v)
      p.survival[t,v,2] <- p.SV1[t,v]

# Sub-process 3: Population length structure #
# Data (m.TMM) are organized by t=year, length (1:5), m=month #
      p.LN[t,v,(1:5)] ~ ddirch(alpha.LN[v,(1:5)])
      m.TMM[t,(1:5),v] ~ dmulti(p.LN[t,v,(1:5)],M.TMM[t,v,1])

# Sub-process 4: Sampling efficiency
# Data (m.FF) are organized by t=year, length (1:5), m=month #
      for (l in 1:5) {
        logit(p.SEL[t,f,l]) <- eta[1]*(l-eta[2])
        iota[t,v,l] <- p.SEL[t,v,l]*p.LN[t,v,l]
        }
```

```
      p.BYP[t,v,(1:5)] <- iota[t,v,(1:5)]/sum(iota[t,v,(1:5)])
      m.FF[t,(1:5),v] ~ dmulti(p.BYP[t,v,(1:5)],M.FF[t,v,1])

      m.FF[t,6,v] ~ dbin(omega[t,v],M.FF[t,v,2])

# Sub-process 5: Subsampling and observation #
# Data (y) are organized by t=year, m=month,f=fish facility #
      for (f in 1:2) {
         gamma[t,v,f] ~ dnorm(G[f],tau.EF[f])
         for (l in 1:5) {
            p.EF[t,v,f] <- p.SEL[t,v,l]*ilogit(gamma[t,v,f])
            n.FF.l[t,v,f,l] <-n.source[t,v]*p.TR[t,v,f]*p.LN[t,v,(1:5)]*p.EF[t,v,f,l]*p.survival[t,v,f]*rho[t,v,f]
            }
         n.FF[t,v,f] <- sum(n.FF.l[t,v,f,(1:5)])

         y[t,v,f] ~ dpois(n.FF[t,v,f]/(1-omega[t,v]))
         }
      }
   }
}
```

1 **Appendix D**

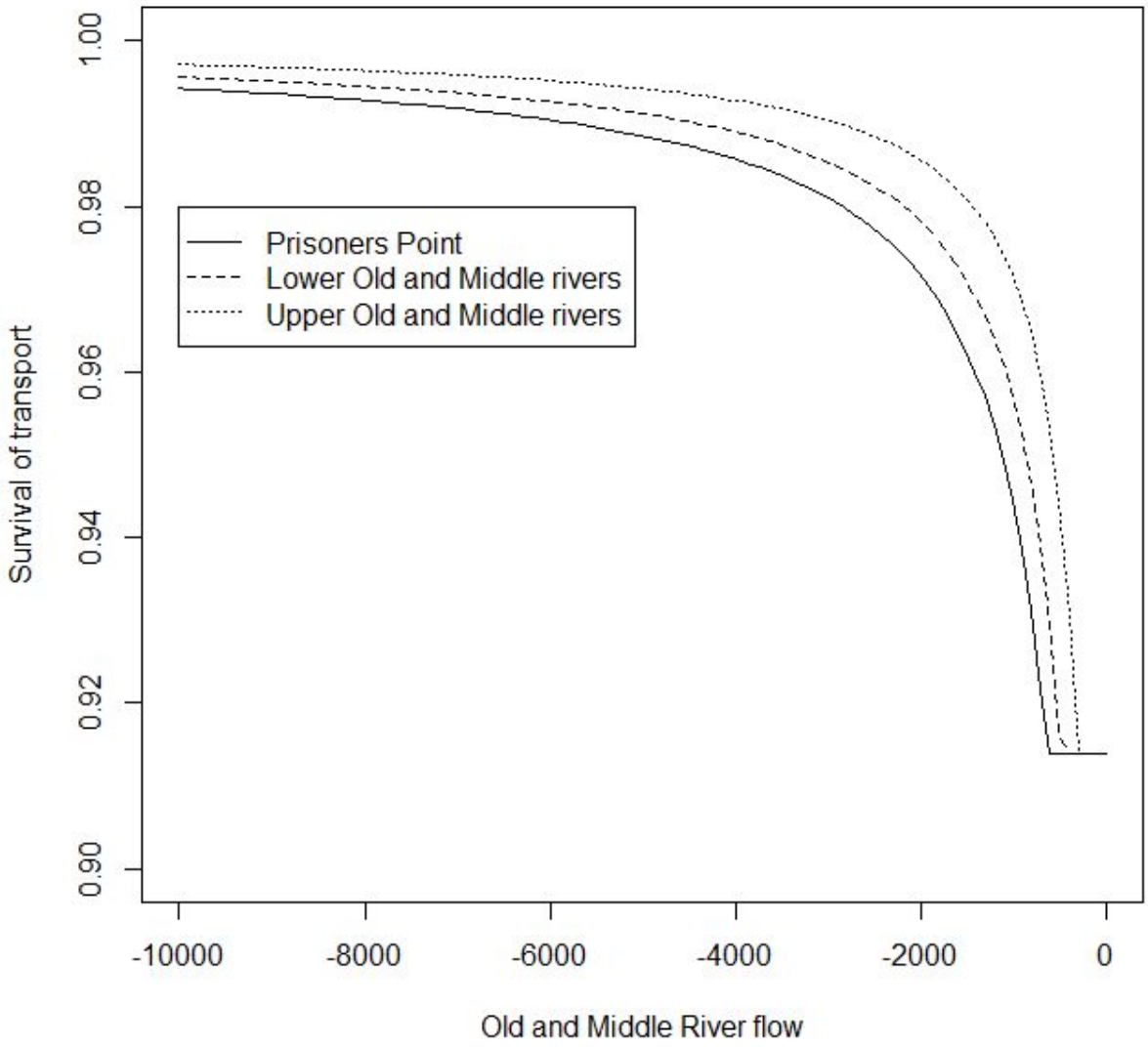

2

3 **Figure D1.** Assumed survival rates p_{SV1_q} from each source region over a range of Old and Middle River

4 flows (cubic feet per second), representing transport times. Survival was truncated at 0.914.

5

Additional diagnostic plots

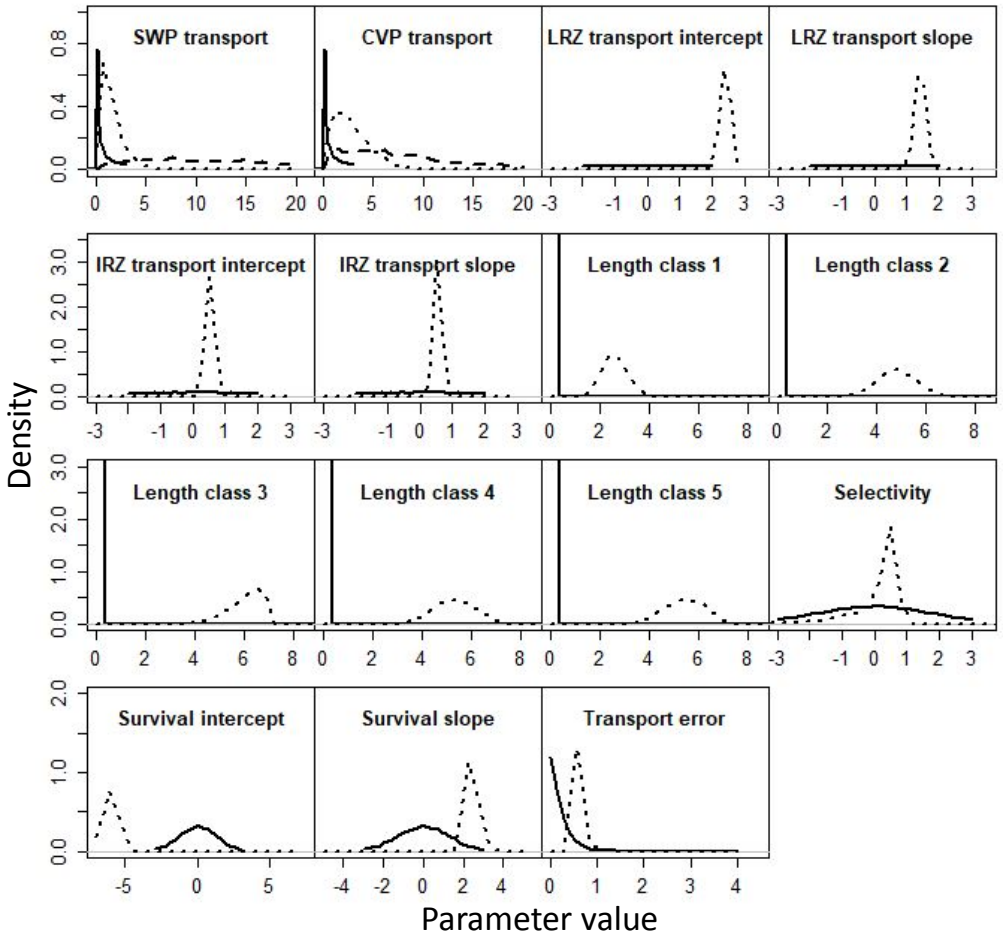

Figure D2. Prior versus posterior distributions for select model parameters. Prior distributions are indicated with the dashed and dotted lines, and posterior distributions are represented with the solid lines. As the model included up to 217 parameters, not all parameters are shown. State Water Project (SWP) and Central Valley Project (CVP) transport parameters for May and June of 2002 and population length parameters for June are depicted as examples. LRZ represents Low Risk Zone parameters, and IRZ represents Intermediate Risk Zone parameters.

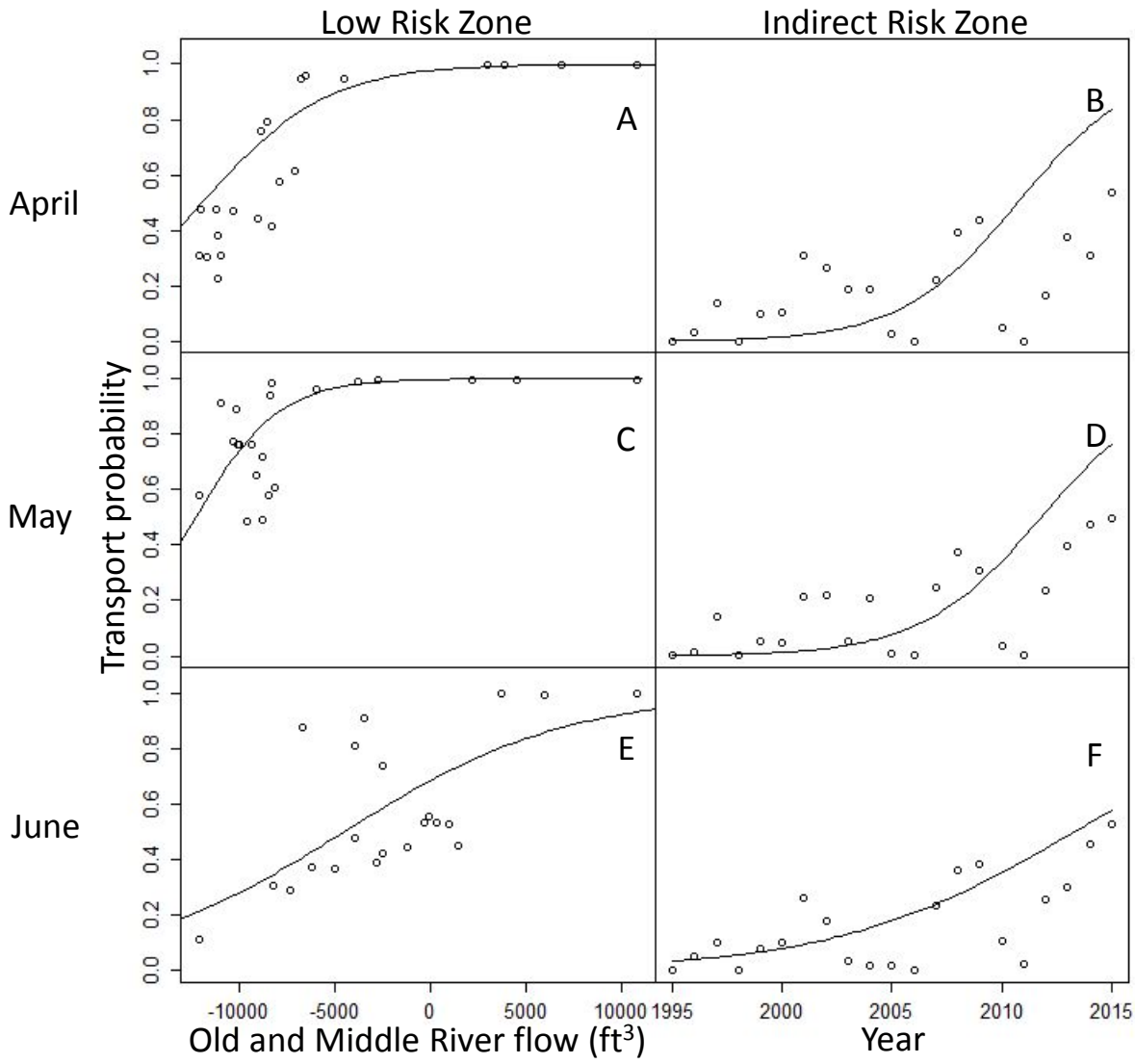

Figure D3. Empirical (particle tracking count/total number of particles) transport probabilities (dots) versus model estimated (lines) transport probabilities for the Low (panels A, C, and E) and Indirect Risk Zones (panels B, D, and F) when the source region was Prisoners Point on the San Joaquin River. Low Risk Zone probabilities were estimated as a function of Old and Middle River flow (Eq. C1), while holding all other probabilities at the monthly median value, and Indirect Risk Zone probabilities were estimated as a function of Old and Middle River flow (Eq. C2), while holding all other probabilities at the monthly median value.

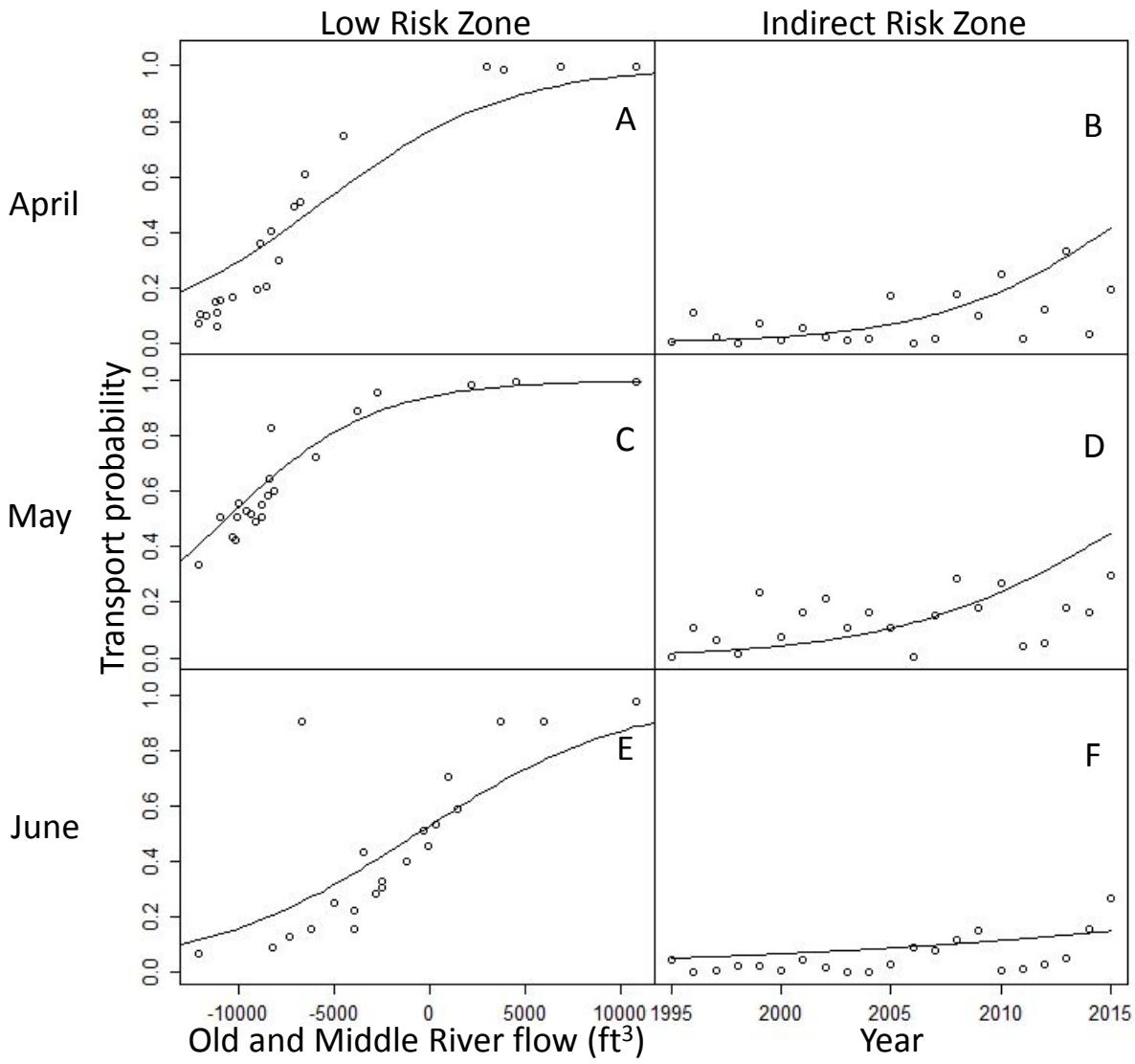

Figure D4. Empirical (particle tracking count/total number of particles) transport probabilities (dots) versus model estimated (lines) transport probabilities for the Low (panels A, C, and E) and Indirect Risk Zones (panels B, D, and F) when the source region was Lower Old and Middle rivers. Low Risk Zone probabilities were estimated as a function of Old and Middle River flow (Eq. C1), while holding all other probabilities at the monthly median value, and Indirect Risk Zone probabilities were estimated as a function of Old and Middle River flow (Eq. C2), while holding all other probabilities at the monthly median value.

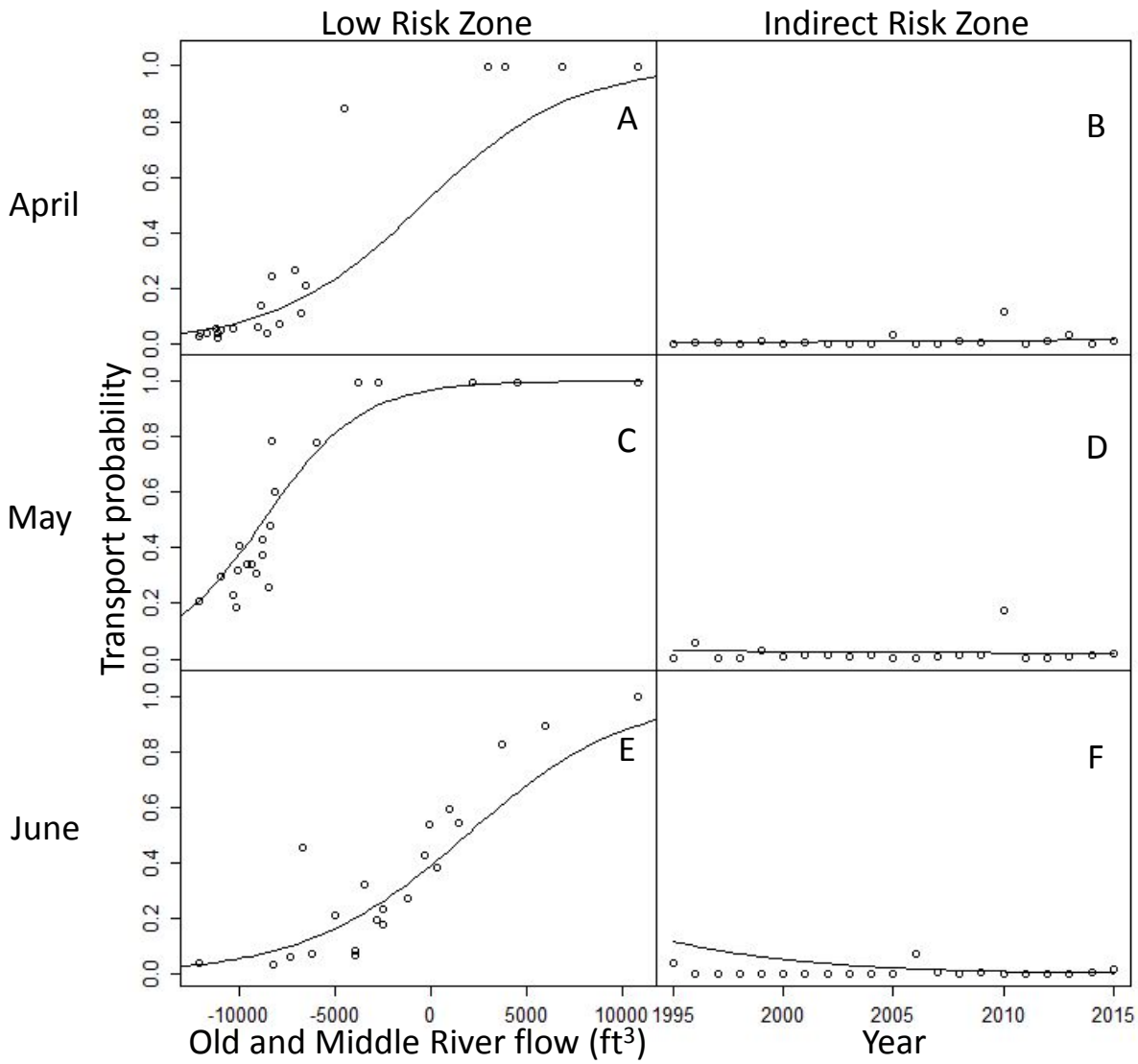

Figure D5. Empirical (particle tracking count/total number of particles) transport probabilities (dots) versus model estimated (lines) transport probabilities for the Low (panels A, C, and E) and Indirect Risk Zones (panels B, D, and F) when the source region was Upper Old and Middle rivers. Low Risk Zone probabilities were estimated as a function of Old and Middle River flow (Eq. C1), while holding all other probabilities at the monthly median value, and Indirect Risk Zone probabilities were estimated as a function of Old and Middle River flow (Eq. C2), while holding all other probabilities at the monthly median value.

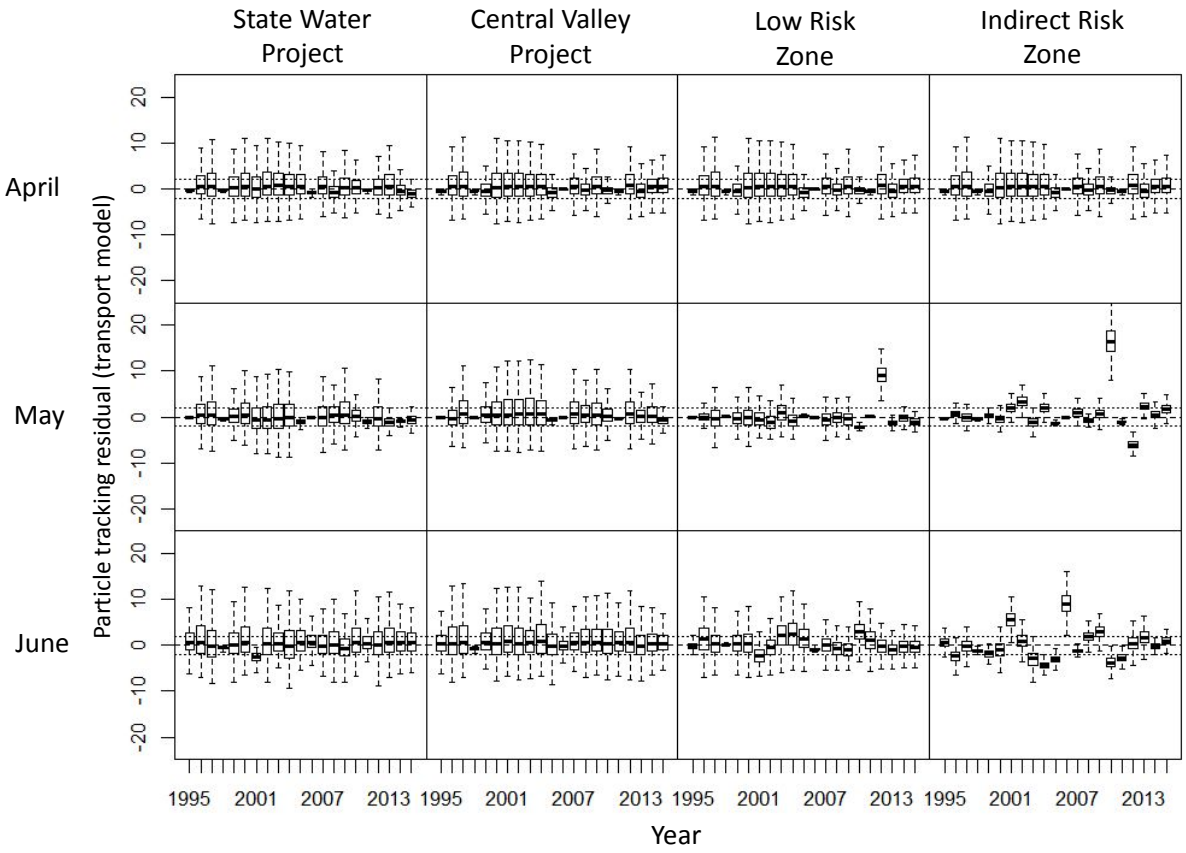

Figure D6. Time series of standardized residuals of the transport model fit to particle tracking data (Eq. 2). Boxplots of posterior residual distributions are shown, and the reference lines indicate the reference values -2, 0, and 2.

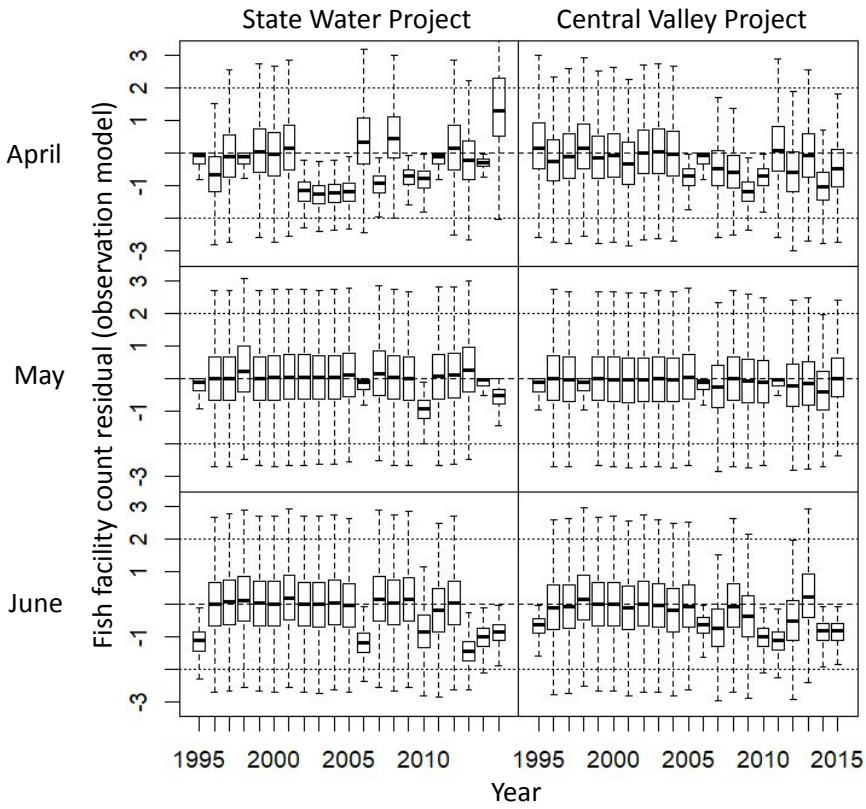

Figure D7. Time series of standardized residuals of the observation model fit to counts at fish facilities (Eq. 13). Boxplots of posterior residual distributions are shown, and the reference lines indicate the reference values -2, 0, and 2.

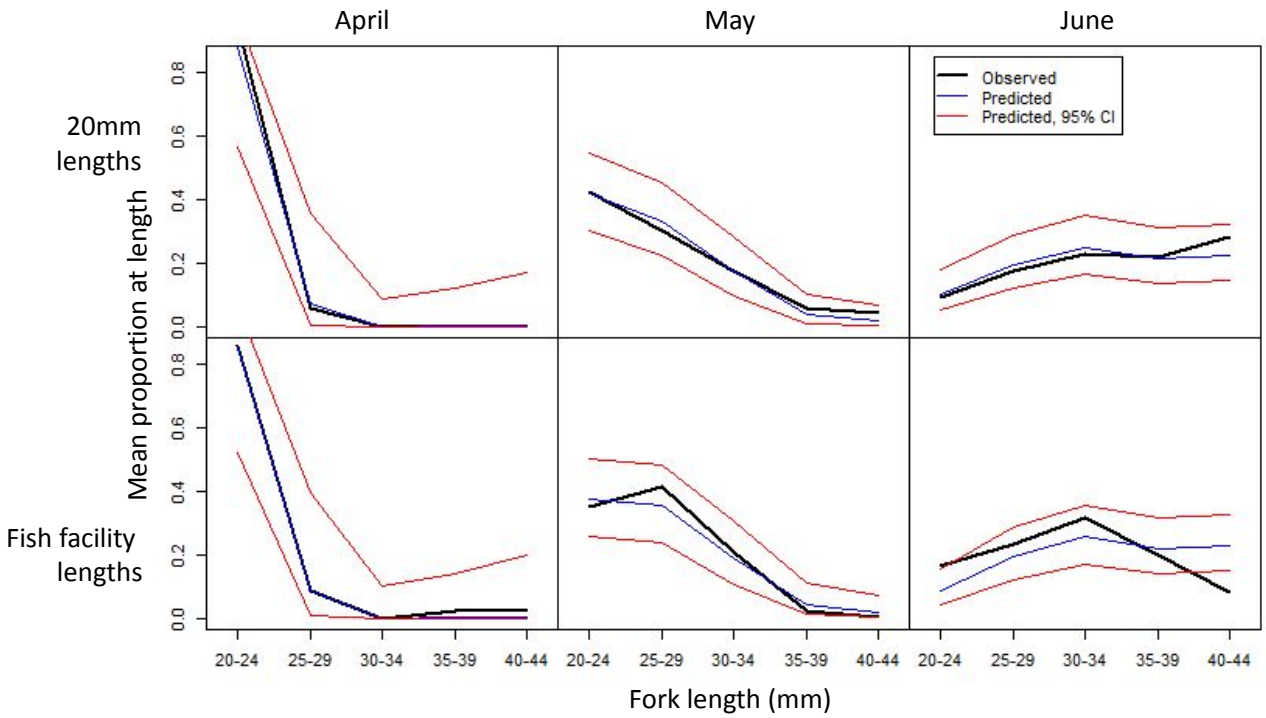

50

51 **Figure D8.** Mean observed (black) versus predicted proportion (blue = mean; red = 95% credible

52 interval) at length from 20mm survey data (p_{LN}; top row) and from lengths sampled at fish facilities (p_{BYP}

53 ; bottom row).